1995-09

Failure site location by acoustic emission for composites reliability assurance

Gish, Donald A.

Monterey, California. Naval Postgraduate School

NAVAL POSTGRADUATE SCHOOL
MONTEREY, CALIFORNIA

TO: Code AA/CO

THESIS

FAILURE SITE LOCATION BY ACOUSTIC EMISSION FOR COMPOSITES RELIABILITY ASSURANCE

by

Donald A. Gish

September, 1995

Thesis Advisor: Edward M. Wu

Approved for public release; distribution is unlimited.

REPORT DOCUMENTATION PAGE

Form Approved OMB No. 0704-0188

1. AGENCY USE ONLY *(Leave blank)*	2. REPORT DATE September 1995	3. REPORT TYPE AND DATES COVERED Master's Thesis

4. FAILURE SITE LOCATION BY ACOUSTIC EMISSION FOR COMPOSITES RELIABLILITY ASSURANCE.	5. FUNDING NUMBERS Grant No. 32384-EG
6. AUTHOR(S) Donald A. Gish	
7. PERFORMING ORGANIZATION NAME(S) AND ADDRESS(ES) Naval Postgraduate School Monterey CA 93943-5000	8. PERFORMING ORGANIZATION REPORT NUMBER
9. SPONSORING/MONITORING AGENCY NAME(S) AND ADDRESS(ES) Engineering and Enviromental Science Division Army Research Office	10. SPONSORING/MONITORING AGENCY REPORT NUMBER
11. SUPPLEMENTARY NOTES The views expressed in this thesis are those of the author and do not reflect the official policy or position of the Department of Defense or the U.S. Government.	
12a. DISTRIBUTION/AVAILABILITY STATEMENT Approved for public release; distribution is unlimited.	12b. DISTRIBUTION CODE

13. ABSTRACT *(maximum 200 words)*

The failure of fiber filaments in a composite subjected to load produces a stress wave which can be detected using acoustic emission techniques. The spatial clustering of multiple fiber failure sites is known to cause catastrophic failure of the macro composite. Acoustic emission can be used to determine locations of these flaws, providing a useful tool for reliability assurance of composite structures. This investigation establishes the necessary foundation by categorically quantifying the methodology of determining flaw locations in a one dimensional solid. Homogeneous isotropic (steel) thin rods are subjected to repeatable wave events to quantify distance measurement, resolution and repeatability. This experimentation is then extended to a unidirectional carbon fiber composite rod with further investigation to quantify effects of dispersion and damping in this heterogeneous, anisotropic material.

14. SUBJECT TERMS Acoustic Emission, Composite Reliability, Composite Failure			15. NUMBER OF PAGES 76 16. PRICE CODE
17. SECURITY CLASSIFICATION OF REPORT Unclassified	18. SECURITY CLASSIFICATION OF THIS PAGE Unclassified	19. SECURITY CLASSIFICATION OF ABSTRACT Unclassified	20. LIMITATION OF ABSTRACT UL

NSN 7540-01-280-5500

Standard Form 298 (Rev. 2-89)
Prescribed by ANSI Std. 239-18 298-102

Approved for public release; distribution is unlimited.

FAILURE SITE LOCATION BY ACOUSTIC EMISSION FOR COMPOSITES RELIABILITY ASSURANCE

Donald A. Gish
Lieutenant, United States Navy
B.S., Tulane University, 1987

Submitted in partial fulfillment
of the requirements for the degree of

MASTER OF SCIENCE IN AERONAUTICAL ENGINEERING

from the

NAVAL POSTGRADUATE SCHOOL
September 1995

Author: [redacted]
Donald A. Gish

Approved by: [redacted]
Edward M. Wu, Thesis Advisor

[redacted]
Gerald H. Lindsey, Second Reader

[redacted]
Daniel J. Collins, Chairman
Department of Aeronautics and Astronautics

ABSTRACT

The failure of fiber filaments in a composite subjected to load produces a stress wave which can be detected using acoustic emission techniques. The spatial clustering of multiple fiber failure sites is known to cause catastrophic failure of the macro composite. Acoustic emission can be used to determine locations of these flaws, providing a useful tool for reliability assurance of composite structures. This investigation establishes the necessary foundation by categorically quantifying the methodology of determining flaw locations in a one dimensinal solid. Homogeneous isotropic (steel) thin rods are subjected to repeatable wave events to quantify distance measurement, resolution and repeatability. This experimentation is then extended to a unidirectional carbon fiber composite rod with further investigation to quantify effects of dispersion and damping in this heterogeneous, anisotropic material.

TABLE OF CONTENTS

ACKNOWLEDGEMENT

The author would like to acknowledge the financial support of the Army Research Office, Engineering and Enviromental Science Division , under Dr. Kailasam Iyer. This work was performed under Grant number 32384-EG.

I would like to thank my advisor, Professor Edward M. Wu for the opportunity and guidance of this work. I would also like to thank Dr. Steven M. Ziola for the generous technical and professional support throughout this investigation. Finally, the greatest appreciation is extended to my mother for all the additional support required while involved in this project.

I. INTRODUCTION

A. NEED FOR RELIABILITY TESTING

Carbon fiber materials are being used in a wide range of applications today. From bicycles to the U.S. Navy's latest fighter attack aircraft, the F/A-18 E/F, this high strength, lightweight material is becoming the choice of designers and builders everywhere. This is especially true in the aircraft and other performance critical communities. Less weight leads to increased maneuverability and greater power to weight ratios. When designing structures to the edge of the strength life envelope, precise information on the structure's ability to withstand the loads encountered is of prime importance. Catastrophic failure, though rare, adversely effects cost and safety. Even on as large a scale as an aircraft, the failure of carbon fiber materials is dominated by local properties of the fiber and matrix bonding. A definitive composite reliability characterization must be pursued to model the failure process behaviour. Coordinated modeling of the failure mechanisms in a mechanics of materials sense and accounting for the sequential failure processes has produced promising probability models. These probability methods form a framework that allows data obtained from laboratory testing samples of small dimensions to be applied to total structures of signifigantly different scale and configuration. Likewise, the proof testing of materials can be applied to manufacturing processes to allow zero reject manufacting of large scale composite structures.(Wu and Bell, 1992)

Analysis based reliability standards are possible only when an extensive data base of material properties is available. This data base is still under development for composite materials. Parametric modeling of the probabilistic representation of the salient failure

processes allows a generic mathematical model for the fiberous material to be developed. Once this model is validated, subsequent specific applications require experimental measurement of the parameters, thereby limiting the effort involved to tractable levels. It is the purpose of this thesis to explore the suitability of using acoustic emission techniques to identify the source locations of fiber failure breaks in a carbon fiber strand which will in turn lend physical support of the load sharing models developed by Rosen, Harlow and Phoenix (1981), Wu et al.

This introduction will continue with a characterization of composite fiber failure and mathematical models. Chapter II, Wave Theory for Thin Rods, will present the mathematical models for theories of wave mechanics in thin rods. Chapter III, Acoustic Emission Source Location, will consider the basic requirements of acoustic event detection in thin rods. Finally, results of Acoustic Emission (AE) source location will be presented in Chapters IV, V, and VI. Specific details of the equipment used in the experimentation and development of parameters for source location software implementation are presented in the appendices.

B. PROBABILISTIC MODELING OF COMPOSITE FAILURE

Uni-directional fiber matrix composites consist of strong, stiff fibers embedded in a matrix of high shear strength material. The fiber-matrix interface gives composites local redundancy in structural integrity. The interface consists of the bond between the fiber and the matrix material. The three types of bonding include chemical, electrical, and mechanical. The scope of this work will not include an investigation into these categories of bonding, but will instead focus on the load transfer mechanism which can be presented

in mechanistic terms. The nature of this interface becomes apparent when it is considered that a 1 in^3 sample of fiber based composite (50% fiber by volume with fibers 0.0003 inch in diameter) contains 6500 in^2 of interface area. Increasing the strength of the interface by using matrix materials of greater shear strength improves static strength, but the fracture mode becomes more brittle.(Chamis, 1974)

Chamis(1974) showed that unidirectional plys fail in 3 main modes: 1) brittle, 2) brittle with filament pullout and 3) staggered failure brittle with filament pull out, accompanied by interfillament matrix shear and constituent debonding.

The two major means of modeling these failures are through either strength of materials analysis or probabilistic modeling. The strength of materials method attempts to quantify the strength of the composite in terms of the constituent materials (fiber and matrix) in a volume fracture weighted approach. The probabilistic method incorporates the statistical strength variations in the individual fibers to the sequential failure and load transfer via the matrix to arrive at a probabilistic strength of the composite.

A single fiber failure within a unidirectional composite under a sustained tensile load is considered. At the broken fiber site, the local load carrying capability of the fiber is reduced to zero. The fiber matrix interface allows shear stresses to form, transferring load originally carried by the broken fiber to the adjacent fibers. This load sharing distribution results in higher stresses for the fibers nearest the broken fiber. This stress concentration diminishes away from the broken fiber site and the global load carrying capability of the composite is preserved.

The sequential failure of multiple sites can be illustrated by views of a composite strand under increasing load level, Figure 1.1. Figure 1.1a is a schematic model of a unidirectional fiber composite under longitudinal tension in the fiber direction. Figure 1.1b is the stress strain curve due to the external loading on the composite as measured directly from the loading/test fixture. Figure 1.1c is a histogram of fiber break locations in the ordinate. The abscissa is the frequency of occurrence of the fiber breaks at the specific spatial length location.

Figure 1.1, illustrates the composite under a mean stress, σ_1. A single fiber has broken, marked by an 'x'. The macro, far field composite stress and strain at the occurrence of this event is illustrated in Figure 1.1b. The single fiber break is tallied at the longitudinal location in 1.1c, marking the start of the histogram of break events.

Figure 1.2 is the same sample under additional load. The higher stress level, σ_2, causes, as an example, two additional fiber breaks. These two breaks are the second and third weakest fiber sites among the entire composite. They may occur along the same fiber lengthwise, as illustrated, because of the load sharing provided by the shear strength of the matrix. These two additional breaks are recorded in the histogram (Figure 1.2c) in their respective lengthwise positions.

Figure 1.3 illustrates the model at a stress state, σ_3. More fibers are broken at various longitudinal positions in the strand. By chance events, a total of two more fiber breaks have clustered in the same general length position. Now the intact fibers in this length position are under a signifigantly higher stress. This produces an increase in the

likelihood for more fibers to fail in this length position, leading to catastrophic failure of the entire composite.

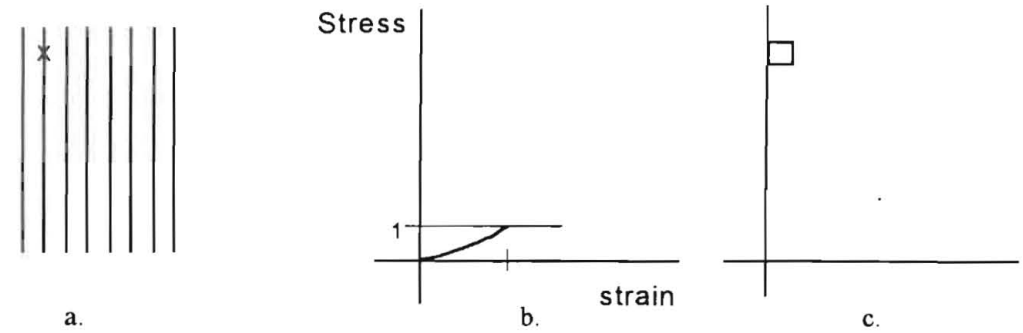

Figure 1.1, Composite Fiber Model

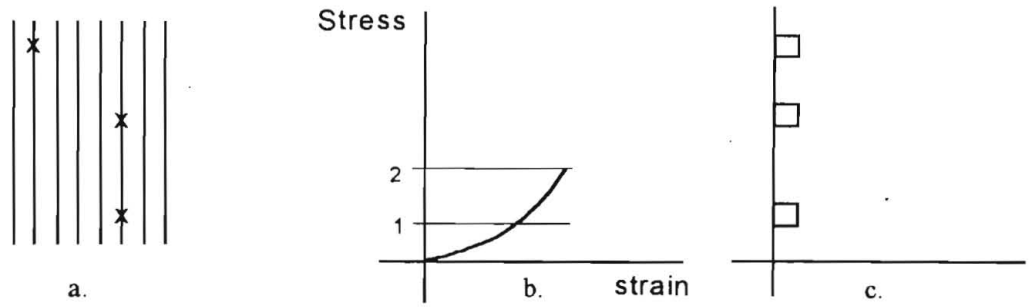

Figure 1.2, Composite Fiber Model

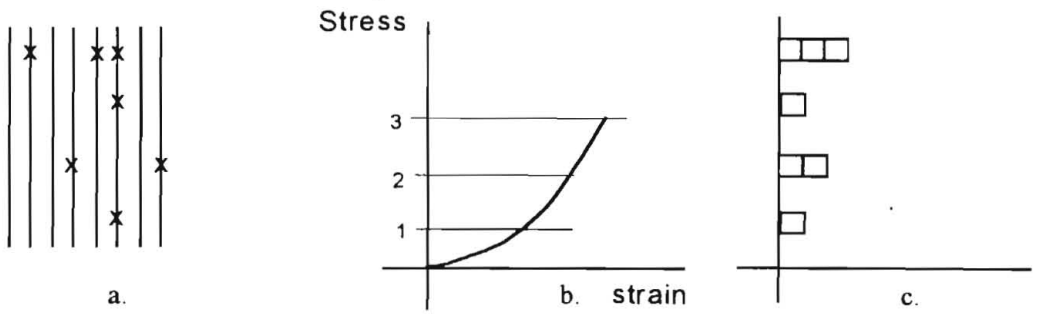

Figure 1.3, Composite Fiber Model

Multiple fiber breaks in the same area of the composite are referred to as clustering. Detection and quantification of clustering is important to the prediction of

composite strength prior to actual failure. Acoustic emission source location will be investigated as a method to detect and quantify the number and location of fiber breaks and the resulting clustering in composites. A long thin composite is used to limit the initial investigation to a one dimensional problem. In the one dimensional problem, only lengthwise clustering needs to be characterized. The composite sample to be considered consists of 1,000 graphite filaments impregnated in an epoxy matrix. This sample is refered to as a strand. The strand is approximately 1 millimeter in diameter and 155 mm in length.

C. FIBER BASED ACOUSTIC EMISSION RESEARCH

Acoustic emission research has been conducted on single fibers. Sachse, et al (1992) showed that a single fiber composite specimen can be treated as a one dimensional waveguide for signals whose dominant wavelengths are greater than any cross sectional dimension. The break locations were determined by using two detectors and a linear source location algorithim. It was shown that for a single fiber, arrival time of the source event for a range of source receiver separations is a linear function of the wave speed. The actual wave speed found was not applicable as it is singular to Nicalon fiber and the matrix used. This approach verifies only wave propagation in single fibers. Location of multiple fiber breaks in the macro scale of the filament (bundle of fibers encased in a matrix material) is required for an understanding of composites behavior.

II. WAVE THEORY FOR THIN RODS

In order to better understand acoustic emission and source location, an understanding of the wave mechanics in thin rods must be considered. The classical theory has been considered by many, but the approach of Kolsky(1963) will be followed here.

In thin rods, three types of vibration can be classified as longitudinal, torsional and lateral. In the longitudinal mode, elements of the rod expand and contract along the length of the rod, with no lateral displacement of the longitudinal axis of the rod. The lateral mode consists of the flexural movement of the bar with the central axis of the bar being displaced laterally. Both these modes are illustrated in Figure 2.1.

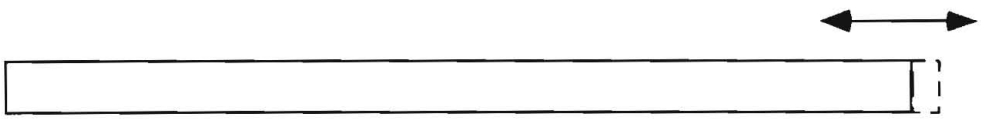

Longitudinal (Extensional) Vibration Mode

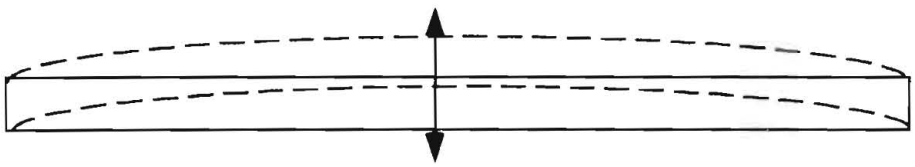

Lateral (Flexural) Vibration Mode

Figure 2.1, Primary Vibrational Modes of Rods

As the previously described fiber break creates a longitudinal stress pulse in the composite, the longitudinal mode is most important to this research. The equations of motion for the longitudinal vibration mode of the thin rod can be derived directly if plane

sections are considered to remain plane and stresses are uniform in the section. Figure 2.2 shows the basic geometry used in the rest of the derivation.

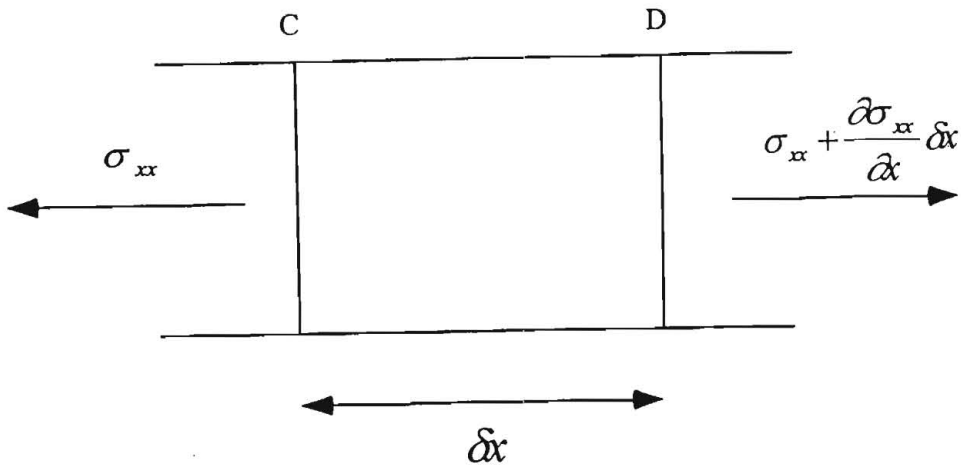

Figure 2.2 Forces Acting on a Rod in Longitudinal Stress(after Kolsky, 1963)

An element of rod, CD, of length δx and area A is considered. The stress on the face of C is σ_{xx} and the stress on the face D is $\sigma_{xx} + (\delta\sigma / \delta x)$. The displacement of the given element is given by u and it's density by ρ. Newton's second law of motion will give:

$$\rho A \delta x \frac{\partial^2 u}{\partial t^2} = A \frac{\partial \sigma_{xx}}{\partial x} \delta x \qquad (2.1)$$

In the one dimensional case, $\sigma_{xx} = E\varepsilon_{xx} = E\frac{\partial u}{\partial x}$, where E is the modulus of the rod. Hence, equation (2.1) can be rewritten as:

$$\rho \frac{\partial^2 u}{\partial t^2} = E \frac{\partial^2 u}{\partial x^2} \qquad (2.2)$$

This is the standard form of the wave equation corresponding to longitudinal waves along a rod with a propogation velocity of $\sqrt{\frac{E}{\rho}}$. The standard form of the solution of (2.2) may be written as:

$$u = f(c_0 t - x) + F(c_0 t + x) \qquad (2.3)$$

Where c_0 corresponds to the wave velocity

$$c_0 = \sqrt{\frac{E}{\rho}} \qquad (2.4)$$

F and f denote arbitrary functions dependent on the initial conditions. The function f corresponds to wave motion in the direction of increasing x. The function F corresponds to wave motion in the opposite direction, or in our experimentation, reflections. This derivation is not restricted to only cylindrical rods, but to any planar geometry.

III. ACOUSTIC EMISSION SOURCE LOCATION

A. ACOUSTIC EMISSION THEORY

Acoustic Emission(AE) is defined as the elastic waves generated by the rapid local redistribution of stresses produced by the damage process. In a composite material, the breaking of a fiber is one of the damage processes that releases energy in the form of a longitudinal wave. A transducer attached to the surface of the composite converts the wave motion to an analog output which can then be captured for further analysis. (Ziola, 1991)

Early methods of AE rely on resonant transducers to capture the wave form. Because the true waveform is altered by the resonant characteristics of the sensor, analysis was typically limited to empirically interpreting the resulting waveform. Parameters such as ring down counts, threshold crossings and amplitude distributions are all attempts to quantify the underlying nature of the event from the altered waveform. Fourier analysis can be used to determine frequency components of the signal. The real part of the Fourier transform is the frequency spectrum, and the absolute value of the transform is proportional to the power spectrum of the signal. However, due to the coloring of the waveform by the resonant sensors, it is not generally successful to identify source mechanisms from this skewed frequency spectrum.(Pao, 1978)

The instrument used in this investigation is the Fracture Wave Detector, model F4000 manufactured by Digital Wave Corporation. This instrument was designed to capture wide band signals of the AE disturbance. The sensors used are high fidelity, wide band transducers. Throughout the frequency band of interest, high fidelity sensors have a

demonstrated true response, without resonant peaks or valleys. A resonant sensor will have a greater sensitivity at its resonant frequency but is significantly less sensitive at all other frequencies(Digital Wave). As the extensional and flexural modes consist of differing frequencies, it is desirable to capture the full wave form without distortions caused by resonancies or colorations of the recording system.

B. SOURCE LOCATION TECHNIQUES

The source (damage process) of a stress wave can be detected by measurement of the difference in arrival time of the wave at transducers of known spatial locations. The difference in arrival times of the wave at different locations is used to triangulate the location of the source by the basic time-speed-distance relation. The distance between sensors is known, as is the speed of wave propagation in the material. The differences in arrival times are determined by the Fracture Wave Detector using two basic algorithims, Threshold crossing and Gaussian Cross Correlation. In the Threshold Crossing method, the arrival time is determined by the time that the AE signal exceeds a pre-assigned voltage threshold.(Figure 3.1)

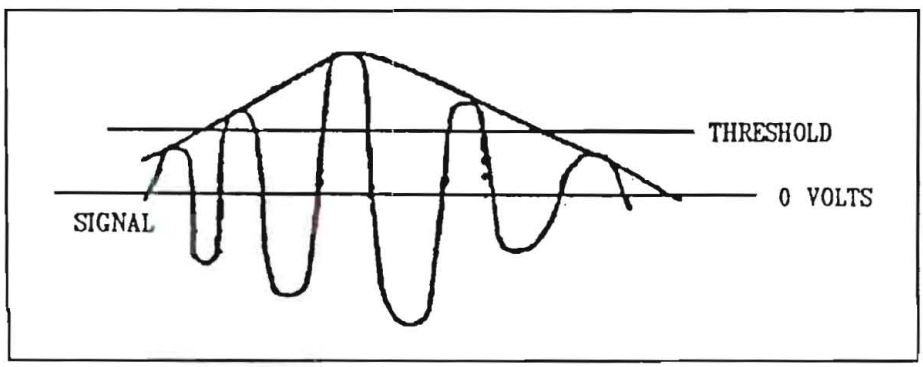

Figure 3.1, Schematic of Threshold Crossing (from Ziola, 1991)

This simple method is accurate as long as the same mode of the wave is being measured at all locations. Pao (1978) noted that the detection of the same first arrived signal by all locations leads to the most straightforward source location. If the first wave is not detectable at all locations, the propagation speed and character of a subsequent wave must be identifiable to produce accurate time difference measurements. Gorman and Ziola (1991) found this to be true in graphite / epoxy coupons. It was found that plate wave propogation consisted primarily of flexural and extensional modes. The extensional mode propagated almost nondispersively, but the flexural mode was highly dispersive. The ability to distinguish between these modes formed the basis for development of the Gaussian cross correlation method. Rather than detecting the first crossing of a voltage threshold, The Gaussian Cross Correlation can locate the arrival time of a specific frequency component of the wave by comparing the captured wave to an amplitude modulated pulse of the desired frequency. Figure 3.2(a) shows the calculated response of the flexural mode in a thin plate, for sources at .305 meters and .610 meters. The modulated cosine is shown in Figure 3.2(b). The two functions were digitally crosscorrelated as shown in Figure 3.2(c). The cursors mark the peaks in the cross correlations and the measured time difference as 131μs.(Ziola, pg 48-49,1991)

As the extensional mode was of greatest interest in this research, threshold crossing was used as the primary means of source location. Lead breaks on the end of a rod produce longitudinal compression waves in the rod. By evaluating the captured waveforms, the extensional character of this wave was found to be relatively non dispersive and able to be measured accurately throughout the bar.

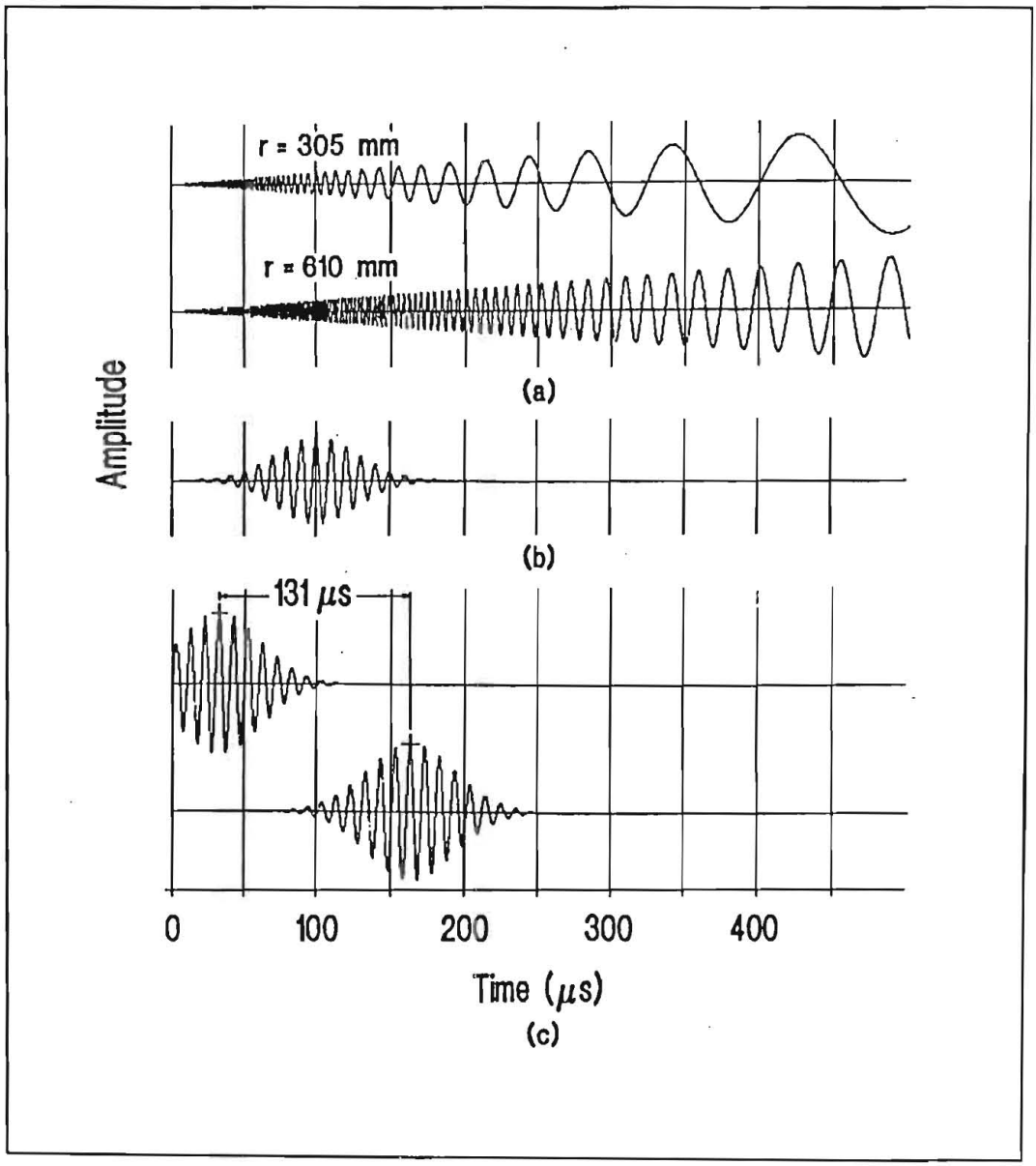

Figure 3.2, Cross Correlation Analysis (from Ziola, 1991)

In the case of actual fiber breaks within a composite sample, the acoustic event will occur between the two transducers of known locations. Arrival times of a known wave component will be determined, and the time difference computed. Using the known speed of propagation in the composite strand and the difference in arrival times, the software can compute the location of the individual fiber break.

In this investigation, series of experiments are designed to characterize spatial resolution, spatial accuracy and repeatability of source location based on acoustic emission. The source event was produced by a lead break performed on the end of the rod. The pencil lead breaks are an accepted method to simulate basic AE characteristics, mainly a step function of known magnitude (Hsu, Hardy, 1978). Other methods of producing an AE event are available. Sachse (1992) used a strain gauge excited by a short duration electrical pulse to excite an AE event for calibration. The breaking of pencil lead with a mechanical pencil has the advantage of being statically applied with a fast release point, producing both perpendicular and parallel surface displacements. In the current experimental configuration, the former produces a flexural wave, the latter an extensional wave. The lead breaks are simple, economical, and convenient to use.

Since the measured event (lead break) occurs outside the transducer, the algorithim provided by the instrument is not capable of computing the actual source location. In the current configuration, the waveform encounters the first sensor, travels the distance between the sensors, then encounters the second sensor. The arrival time difference is simply the time it takes the wave to travel the known distance between the sensors. The software computes the source location at the first transducer encountered.

By assigning the farthest transducer a location of 0 and the first encountered a known distance, variations from the known distance can be tracked as a measure of accuracy.

IV. PRELIMINARY INVESTIGATIVE TESTING

A. ARRIVAL WAVE FREQUENCY

Lead breaks were used to generate a stress wave at the end of the 3/8"diameter isotropic, steel, round rod sample to identify the important frequencies to be recorded and analyzed. The frequency of the arrival wave was computed using the Digital Wave's manual cursor to determine the first wave's period, then its' wavelength. Using this method, hardware band pass filters were set to filter out low frequency noise. In the case of the 3/8" rod, the frequency of the arrival wave was found to be on the order of .14 Mhz (140 kHz). The lower frequencies of the acoustic signal were filtered out using the hardware band pass filter set to a high pass of 0.05 mHz (50 kHz). This was judged to be capable of capturing all relevant wave information, but filtering out low frequency noise.

For comparison, an acoustic event was generated by a Pentel brand, 0.3 mm, 2H lead pencil break at the cross sectional center of the bar. Measurements were taken with the transducer pair 0.05 meter (50 mm) and 0.1 meter (100 mm) from the acoustic event. The transducers were arrayed symmetrically about the rod, as illustrated in Figure 4.1, with 0.1 meter measurement position shown.

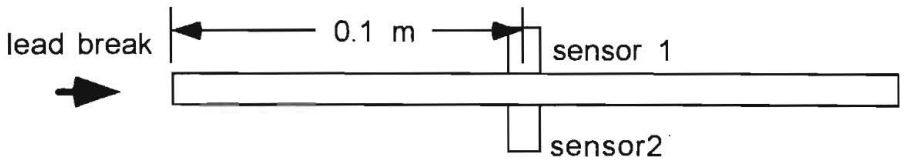

Figure 4.1, Symmetrical Transducer Orientation

One channel recorded the full waveform, the other was filtered as described above. The filtered and unfiltered waveforms taken from transducers located symmetrically about a

steel rod sample, 0.5 meter(50 mm) from the event are presented in Figure 4.2. It can be seen that there is very little difference in the recorded waveforms. The 3/8" steel rod exhibits a wavefrom that is not solely a function of the extensional and flexural modes. There appears to be several higher order, non dispersive mode shapes present, which make analysis difficult.

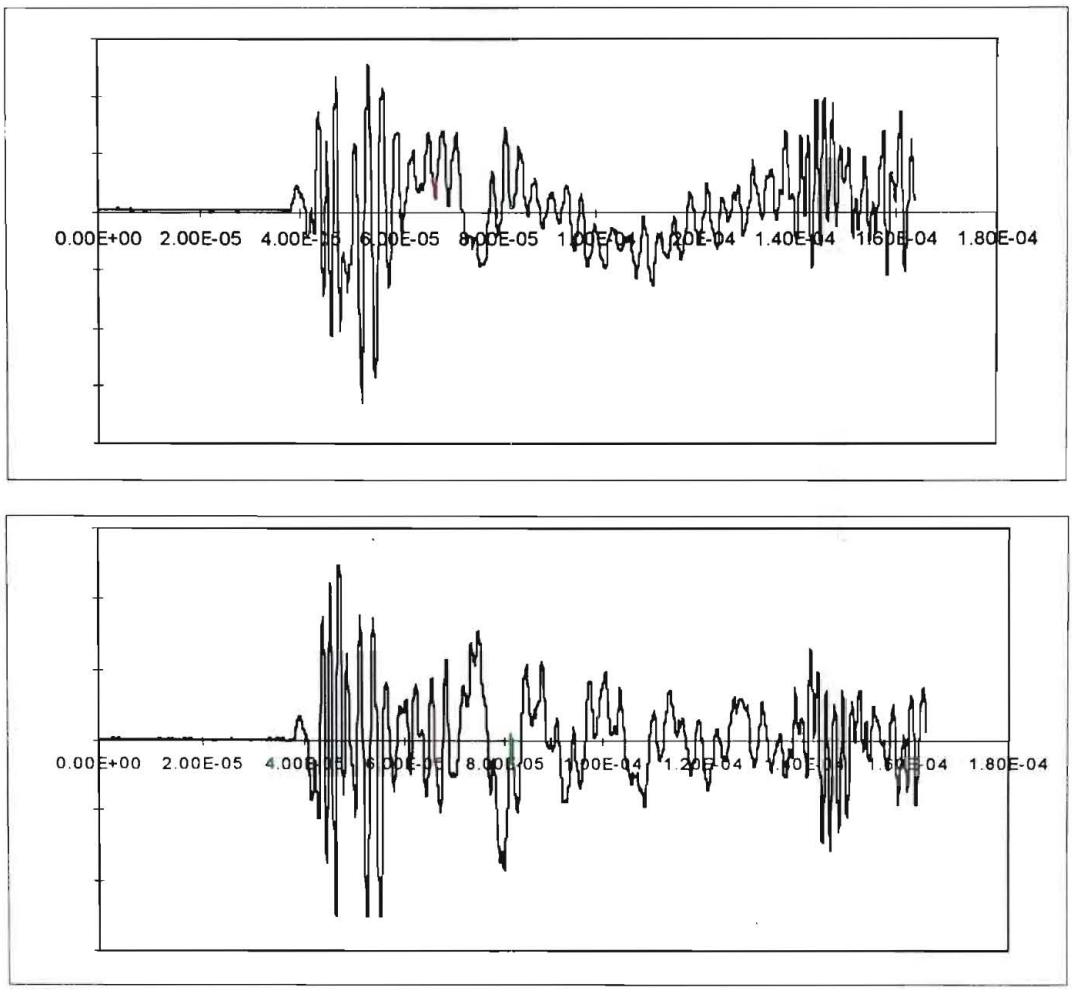

Figure 4.2, Unfiltered (top) and Filtered Waveforms, 0.05 meter from source event

Figure 4.3 shows another set of waveforms, captured 0.10 meter from the acoustic event. Again, one channel recorded the full waveform while the other was filtered.

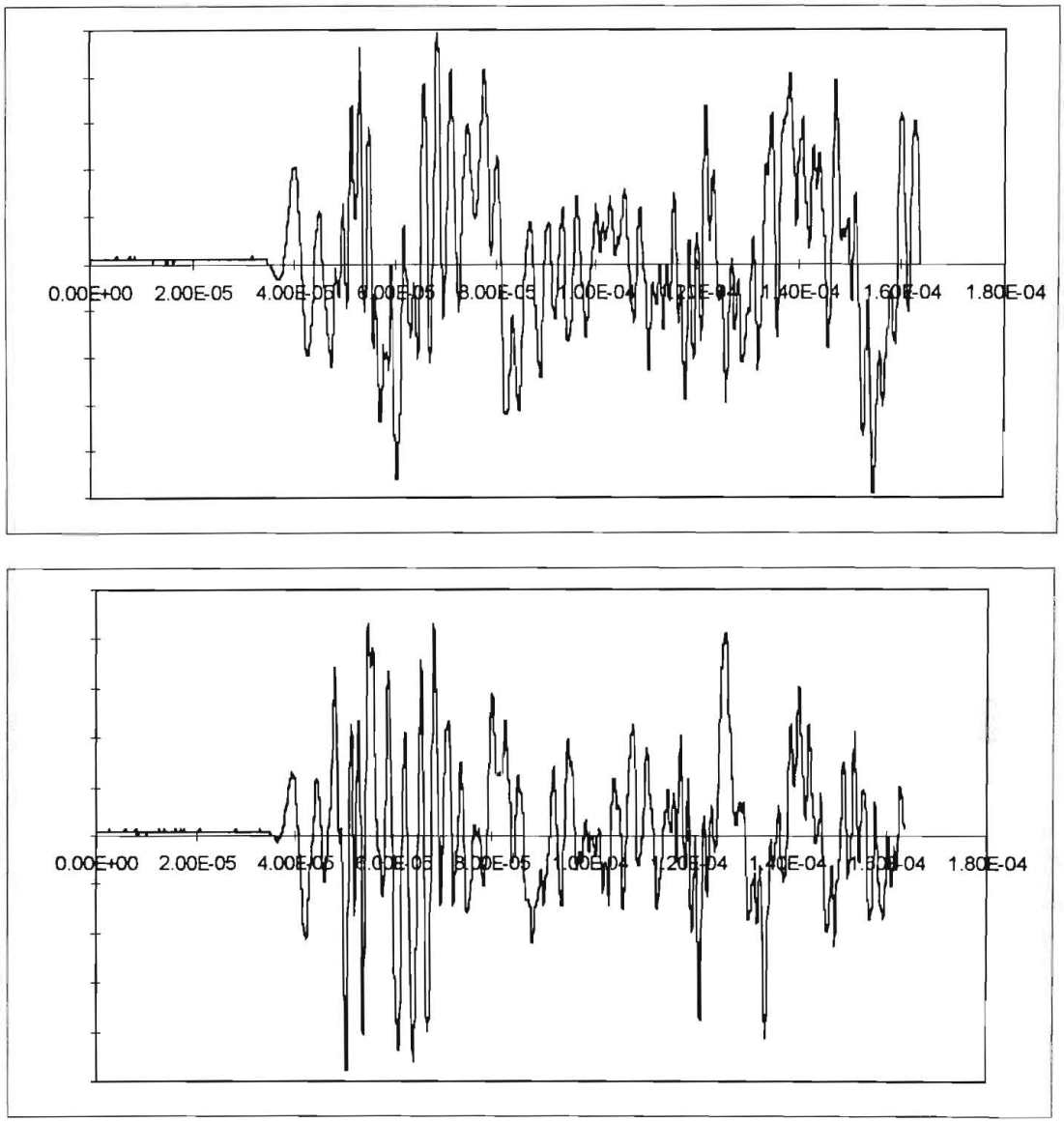

Figure 4.3, Unfiltered (top) and Filtered Waveforms, 0.1 meter from source event

Comparison of Figure 4.2 and 4.3 reveals very little attenuation of the wave signal over the 50 mm difference in measurements. As mentioned earlier, the waveform consists of several modes, but the arrival wave is clearly extensional. Although not obvious from the diagrams, closer investigation using software shows the extensional arrival wave to be

mildly dispersive in the presented case. The magnitude of frequency change is not signifigant enough to effect accuracy at this point. The extensional wave's minimal dispersion and adequate signal strength permit accurate use of the threshold crossing technique for distance measurement.

B. MEASUREMENT OF LONGITUDINAL WAVE

Initial experimentation was conducted to determine the sensitivity of the system to the extensional (longitudinal) waves when measured from the surface. This is important because the fiber breakage in a unidirectional composite produces a compression wave along the axis of the fiber. The optimal location to mount a sensor is at the end surface of the sample, perpendicular to the flexural wave since the sensor is sensitive to displacement normal to the sensor contact surface. Conversely, a sensor mounted on the surface is more suited to detection of flexural waves. In the case of an extensional wave, the parallel side surface mounted sensor detects the Poisson effects of the compression wave. Since the Poissson ratio is approximately 1/3, the sensitivy of the side surface mounted sensor is reduced by a factor of 3. This is illustrated in Figure 4.4 and 4.5, below.

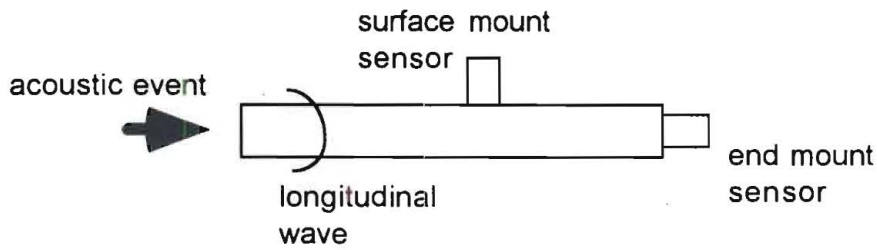

Figure 4.4, Detection of Extensional Waves

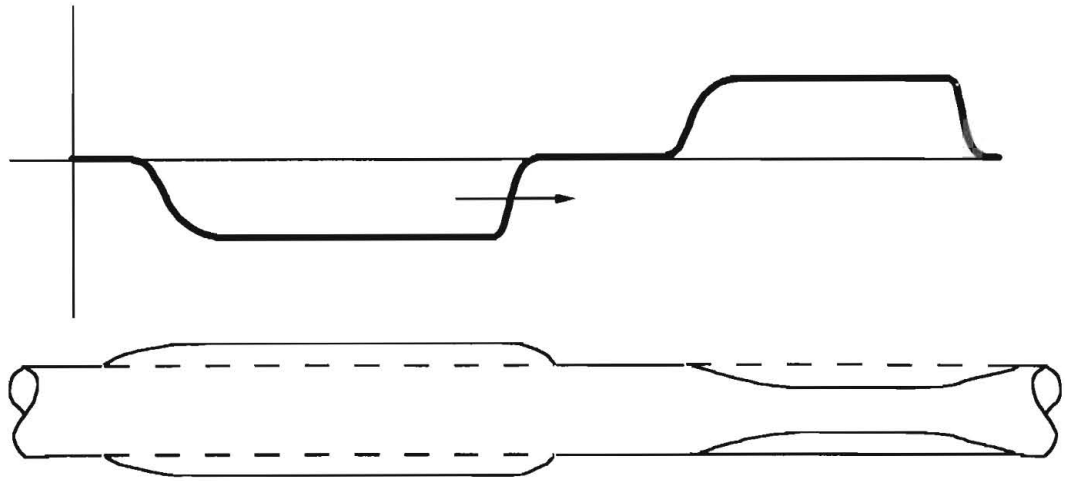

Figure 4.5, Poisson Effect from Longitudinal Stress Pulses(from Graff, 1991)

Because the source of the wave (fiber break) is longitudinal, the ideal mounting of the sensors would be on the end of the samples. Several factors may preclude this ideal mounting position. For load application, the specimen will be mounted in a tension testing fixture of an Instron test machine during recording of the acoustic events. The ends of the fiber specimen are encased in a thermoplastic tab to permit uniform load transfer from the machine's gripping jaw. This tab prevents an end mount transducer from contacting the actual fiber. In addition, the mounting jaw could impart noise to the sample between the actual source and the recording. Side mounting the transducers between the test gauge section will isolate grip and machine noise and is more expedient in implementation of the testing. However, side mounting incurs the penalty of lower sensitivity due to the Poisson effect. This is the configuration pursued in this investigation.

The initial series of tests were conducted on a 3/8"diameter hardened steel rod to determine the effects of end and side mounting of transducers on rod samples. The size of the rod was matched to the diameter of the transducer to allow maximum transmission of

energy to an end mounted transducer. The acoustic source for all these experiments was created by a 0.3 mm 2H Pentel mechanical pencil lead break on the end of the rod sample. Care was taken to produce a stress pulse as near to the center of the rod as possible so as to minimize flexural components of the stress wave. Experiments were conducted to demonstrate that the system was capable of detecting the Poisson induced effect from a longitudinal wave and that the waveform was symmetrical, that is the radial position of the transducer on the bar had no effect on the waveform recorded. Recorded waveforms were presented in Figures 4.2 and 4.3 in the section on filtering. This configuration was shown previously in Figure 4.1.

Transducers were then mounted on the side of the bar at a distance of 0.1 meter to demonstrate that the system was capable of determing distance based on the Poisson induced effect from a longitudinal wave. This is illustrated below in Figure 4.6.

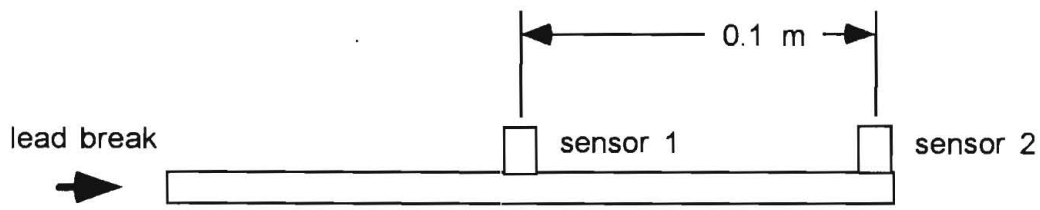

Figure 4.6, Detection of Poisson Components of Longitudinal Wave

At this point, preliminary checks were conducted to ensure threshold crossing techniques accurately measured distance. The stress wave experiment was repeated 40 times by subjecting the sample to lead breaks. The resulting waves were recorded by the Digital Wave Fracture Wave Detector as described in Appendix A. The distance between the sensors was computed using the Digital Wave threshold crossing technique.

Threshold voltage was 0.02 volts, with a wavespeed of 5300 meters / second. The average distance was 99.78 mm, within 1 percent of the measured.

Using the baseline distance measuring results from the above experiment, comparisons were made to determine if measurement differences existed between the poissonal components and directly measuring the longitudinal component. This was accomplished by placing the second sensor at the end of the bar to directly measure the extensional wave. This configuration is shown in Figure 4.7

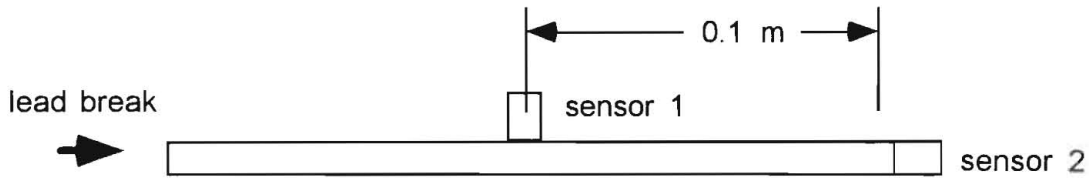

Figure 4.7, End and Side Mount

Again, 40 lead break stress waves were generated and the results analyzed using threshold crossing techniques. Threshold voltage and wavespeed remained as before, but the measured distance used was .105 meter (105 mm). This was the actual measurement from the center of sensor 2 to the end of the rod. The average distance computed using the software was .10581 meter, which is within 1 percent of the expected.

To determine if this .005 meter (5mm) difference was solely an effect of the transducer orientation, the sensors were located together at the end of the bar as shown below in Figure 4.8. This allowed direct measurement of the measurement error between the two previous configurations.

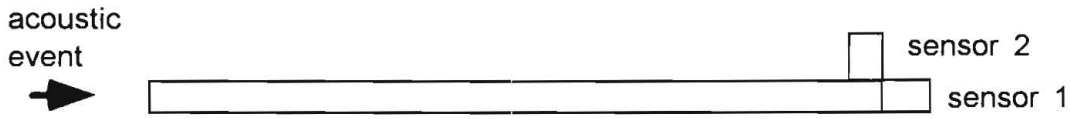

Figure 4.8, End Effect Measurement

Forty lead break events were performed on this configuration. Threshold crossing parameters were unchanged and the measured distance was input as 0.005 meters (5 mm). This measure is approximately one half the diameter of the transducer. Average computed distance was 0.00396 meters (3.96mm), an error of approximately 20 percent. This is a relatively large error measured over a short distance. It is therefore felt to represent the resolution of the side mounted transducer in detecting longitudinal waves.

Mounting the transducers on the side of a 3/8" steel rod provides a sufficent signal sensitivity to capture the extensional wave produced from the acoustic event of a lead pencil break. Using threshold crossing, the measurement of source location has a resolution of between 0.003 and 0.004 meter (3 to 4 mm) and an accuracy of 0.006 meter (6 mm). As the diameter of the transducer is approximately 0.01 meters (10 mm), the histograms of spatial location measurements from further experiments are presented for the measured distance, plus or minus 0.008 meters in 0.001 meter (1mm) intervals. This displayed interval allows for measurement within the resolution of the sensor.

V. RESULTS OF SOURCE LOCATION IN ISOTROPIC MATERIALS

A. EXPERIMENTAL METHOD

To determine the ability of the software to accurately measure distances, a series of experiments was devised. As the signal from an acoustic event arrives at either transducer (2 channel, 1 dimensional measurement) the recording is activated and the signal from both channels are recorded using a common time scale. The software determines arrival times based on a user set voltage threshold and computes the difference in arrival times. Using the known location of the sensors and basic time speed distance calculations, the software determines the location of the source. Since the event occurs outside the transducer, the software computes the location at the first transducer encountered. By assigning the farthest transducer a location of 0 and the first encountered a known distance, variations from the known distance can be tracked as a measure of accuracy.

B. RESOLUTION OF SOURCE LOCATION

The first experiments were formulated to determine the ability of the Digital Wave software to accurately determine distance, that is resolution. Also important was the capability of the software to consistently measure that distance. This is referred to as repeatability. To measure resolution and repeatability, 3 distances were measured: 0.050, 0.10 and 0.150 meter (50, 100 and 150 mm). The configuration of the test sensors is shown below in Figure 5.1.

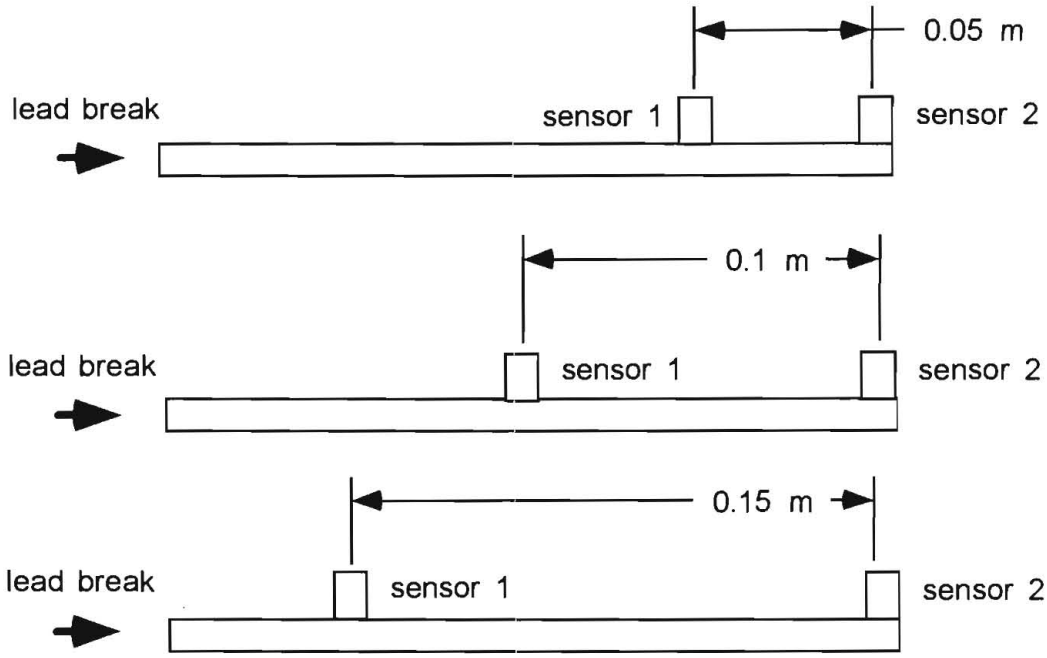

Figure 5.1, Resolution and Repeatability Tests

Forty acoustic events (lead breaks) were recorded for each of these configurations. The Digital Wave threshold crossing software routine was performed on each set of data using a voltage threshold of 0.02 volt. The speed of wave propagation for steel was determined from Digital Wave's software database as 5300 meters/second. This value was considered adequate for early testing and was adjusted as necessary in later testing. The results of the forty events were tabulated using a probability density function created in the Microsoft Excel spreadsheet program.

The density function spreadsheet computed the number of samples within a specified range. For the purposes of distance resolution, samples were grouped within plus or minus 7 millimeters of the known distance, in one millimeter groups. This range of measurement was based on the transducer's diameter of approximately 10 mm. The range

of measurement allows for accuracy within the diameter of the sensor, plus or minus 2 mm. Results of the distance resolution tests are presented graphically for the 3/8" rod in Figure 5.2.

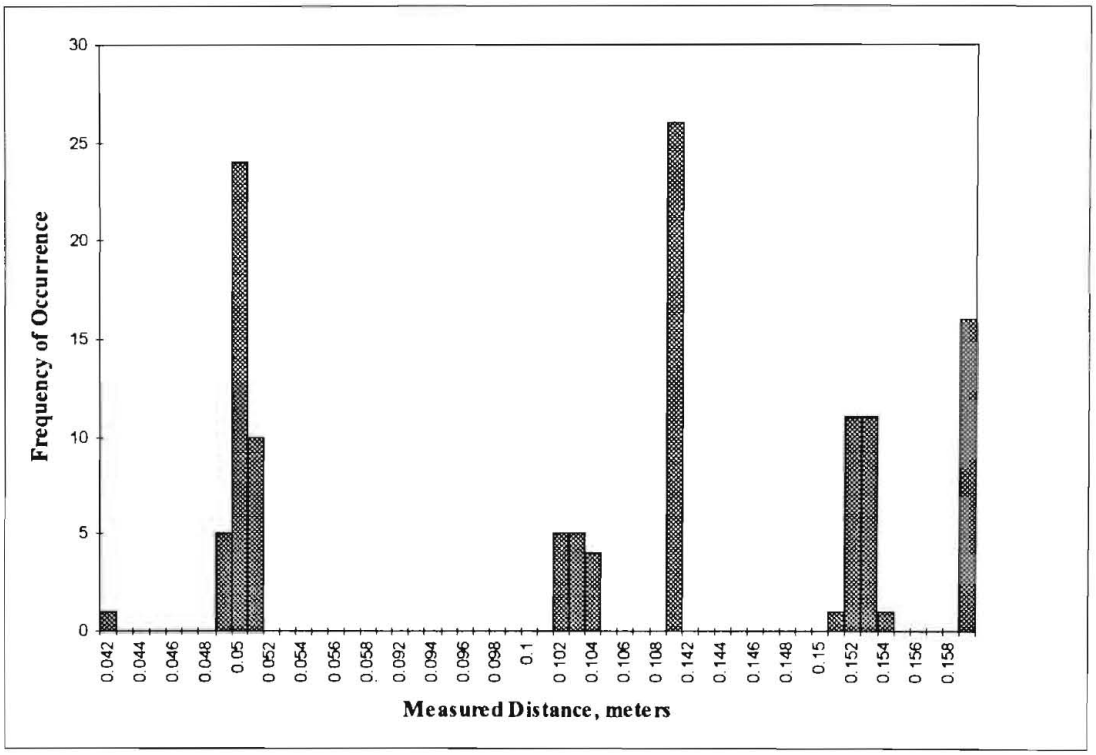

Figure 5.2, 3/8" dia. Steel Rod, Threshold Crossing, 5,300 m/s

In addition to a plot of the raw data, the measurements are presented standardized to the smallest, 0.50 meter measurement. 0.10 meter was subtracted from the 0.15 meter measurement and 0.05 from the 0.10 mm measurement. This allows comparison of the measurement errors on a similiar scale, without scaling effects brought on by division to normalize the data. This standardized data is presented below in Figure 5.3.

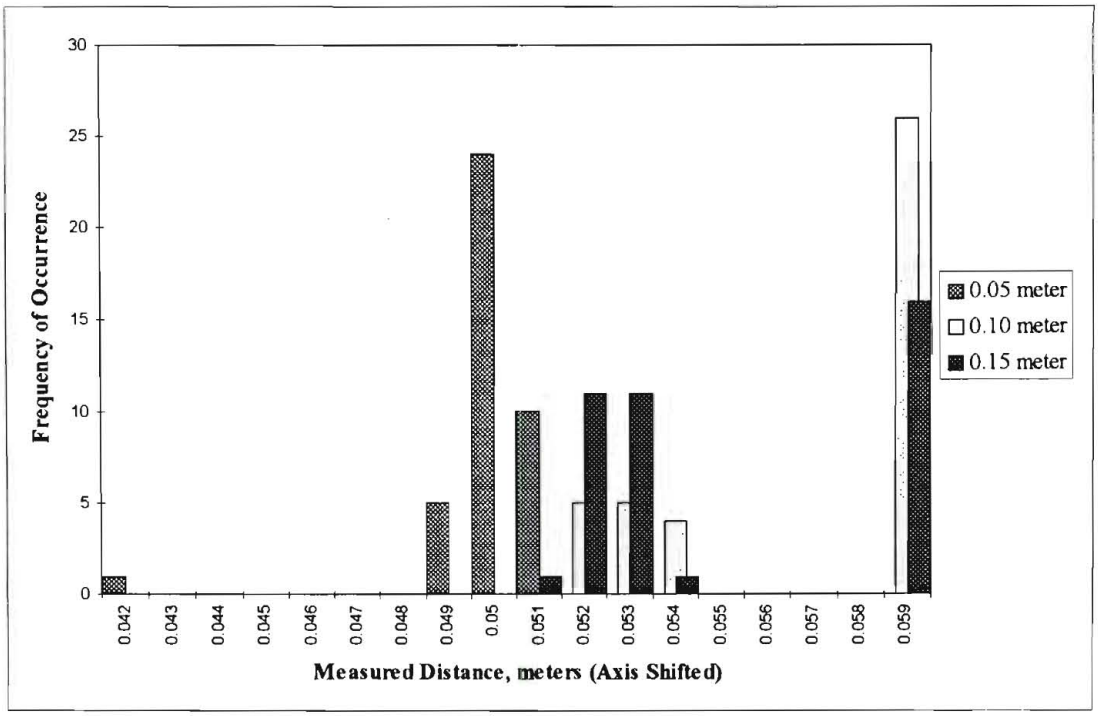

Figure 5.3, 3/8" dia Steel Rod, Threshold Crossing, 5,300 m/s (Standardized)

The standardized graph of distance resolution shows that resolution in the short distance, 0.05 meter (50 mm), is within 0.001 meter (1 mm) of the measured true distance. As the measured distance is increased to 0.1 meter (100 mm), less than 25 % of the samples are within 0.004 meter (4 mm) of the measured value. Likewise the measurement of the 0.15 meter (150 mm) is accurate in over half the events to within 0.004 meter. Since the longest two measurements are actually skewed to a higher mean, it would appear that the signal is actually dispersing enough to affect the distance measurement. That is, lower frequency arrival waves are being measured in the 0.15 meter sample than those measured in the 0.05 meter sample. However, it is not felt that this effect would account for the large number of samples that are beyond the regarded resolution (0.008 meters).

In an attempt to account for the effects of the apparent extensional wave dispersion, the Digital Wave software routine using Gaussian cross correlation was applied to the set of results from the same 3 samples. Results were completely unreliable with computed distances ranging from 0.025 meter to 0.10 meter in the 0.05 meter test. Ziola (1991) had great success using the Gaussian cross correlation technique to measure distance in isotropic plates. The apparent reason for the errors in the case of the 3/8" rod was the many modes present in the recorded waveform (Figures 4.2 and 4.3). Ziola's tests on flat isotropic plates consisted of surface pertubations on flat plates vs the end pertubation utilized here. This surface pertubation produced primarily flexural components, with small amplitude extensional components and very few additional modes. The small amplitude extensional mode was attenuated rather quickly. Since the higher frequency extensional mode was present in some waveforms, but not in others, the difference in detected waves required the cross correlation technique to establish a common waveform. In the rod case the primary mode is the extensional mode and does not appear to attenuate as quickly. The flexural mode is also present with several other non dispersive modes, presenting many possible correlations in a single waveform. The strong extensional wave form was not attenuated and consistently the arrival wave. The extensional wave was adequate for resolution of the measured distance in the initial case.

The resolution dependence on distance was tested in the 1/8" hardened steel rod sample in the same manner. Wave propagation speed used in the threshold crossing routine was still 5300 meters/second. Results were plotted both as distances and standardized as shown in Figure 5.4 and Figure 5.5.

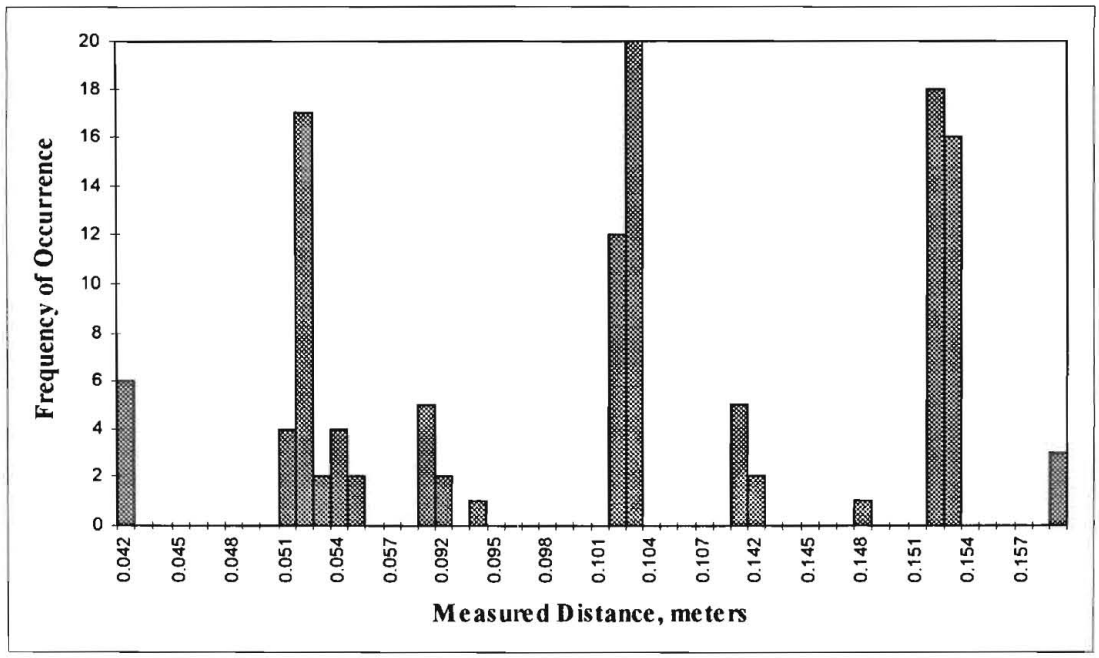

Figure 5.4, 1/8" dia Steel Rod, Threshold Crossing, 5,300 m/s

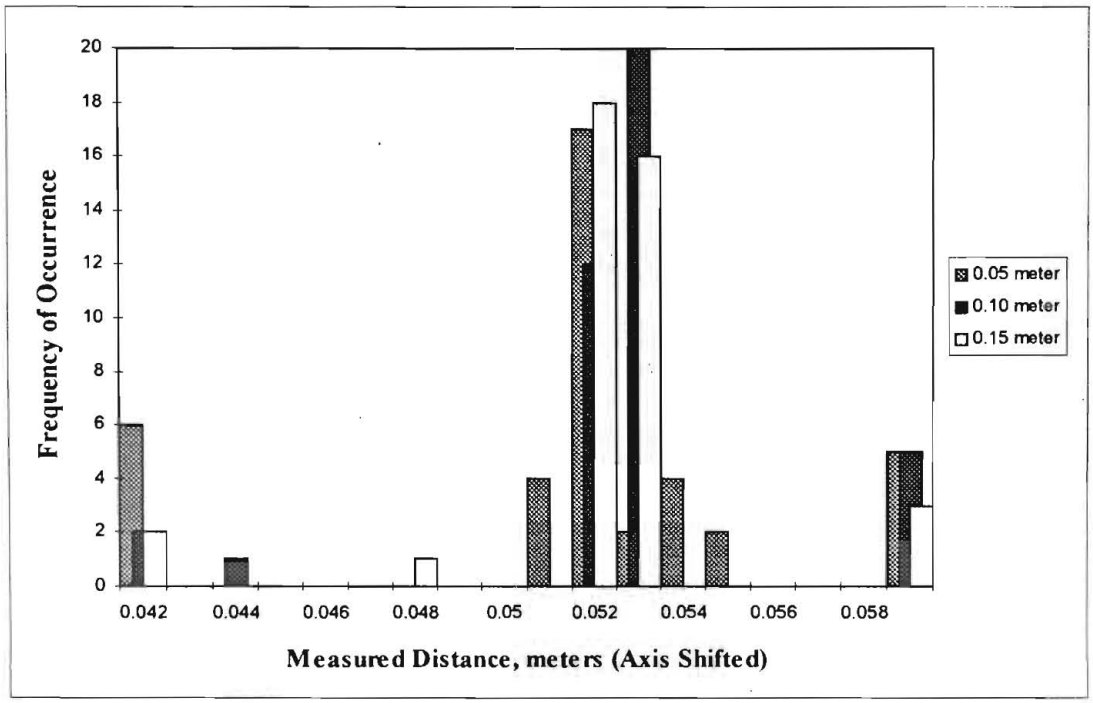

Figure 5.5, 1/8" dia Steel Rod, Threshold Crossing, 5,300 m/s (Standardized)

It can readily be seen comparing Figure 5.5 to Figure 5.3 that the resolution in the 1/8" rod is signifigantly better than in the 3/8" rod. By examining the actual recorded waveforms, this can be attributed to the absence of as many higher order modes in the thinner rod. An example waveform from the 1/8" steel rod is compared to the (filtered) waveform from the 3/8" steel rod (previously presented as Figure 4.2) in Figure 5.6.

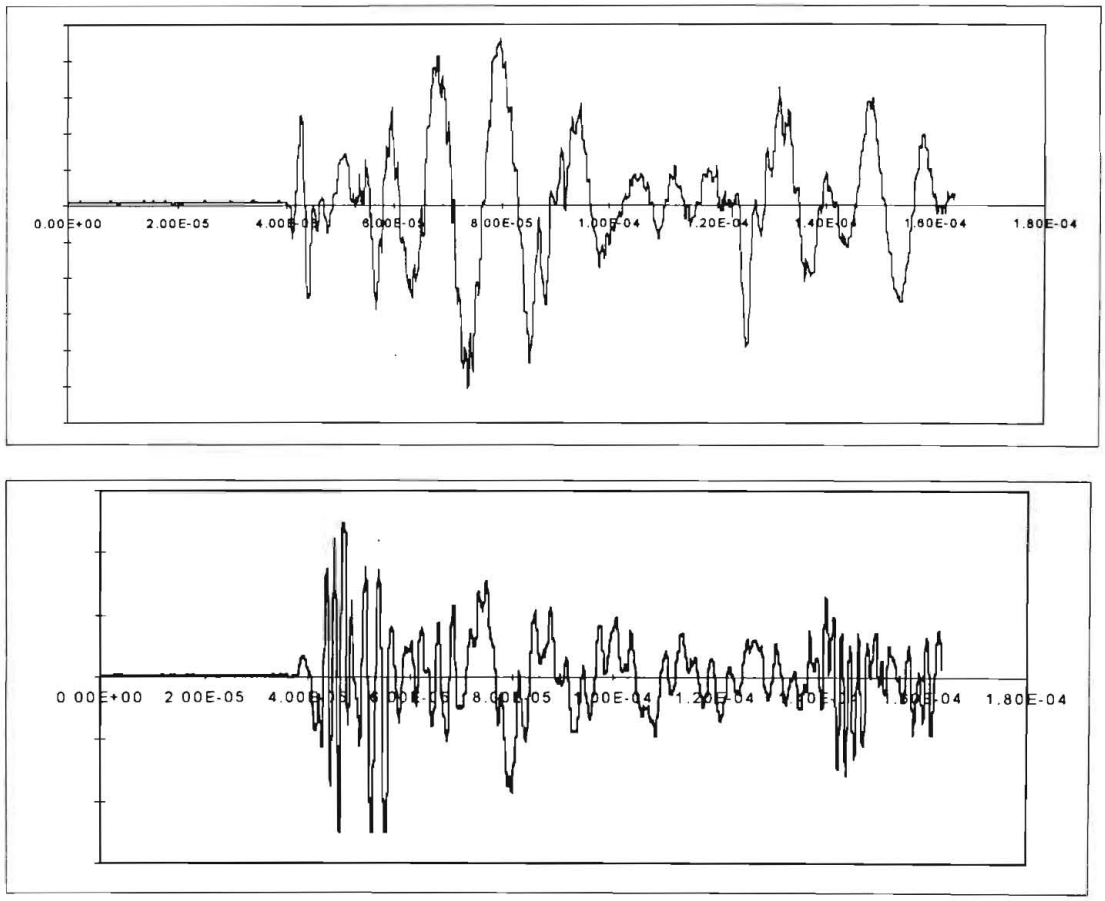

Figure 5.6, Example Waveform in 1/8" Steel Rod, Measured at Center of Rod (top) compared with 3/8" Steel Rod (bottom)

The thin rod more closely approximates the ideal with predominately extensional and flexural waveforms present.

As the apparent mean was centered at approximately 0.052 meter vice 0.50 meter, the threshold crossing alogrithim was used to reinterperet the data, optimizing the central tendency by adjusting the wave speed to 5146 meters / second. This new value was determined by considering 5300 meters / second to be 103 percent of the desired value and solving for the new, desired value. This value does not produce perfect results in this resolution test, but is the best compromise between the resolution and dispersion results discussed later (Figure 5.10). The resulting data using this revised velocity are presented only in standardized form, in Figure 5.7.

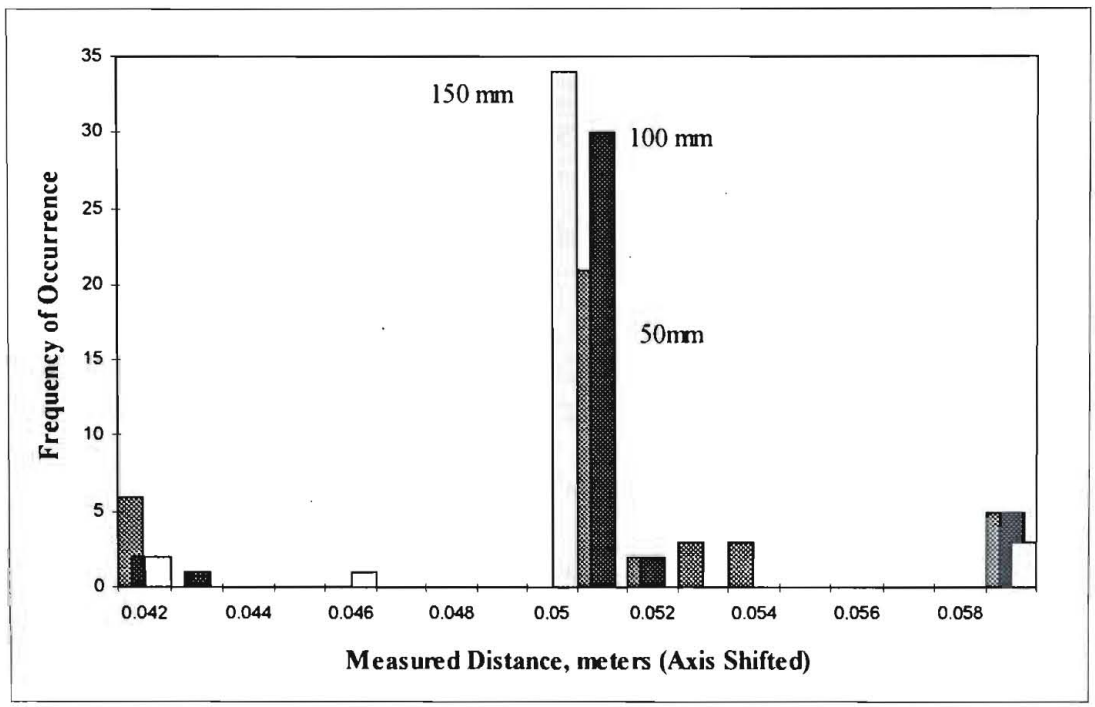

Figure 5.7, 1/8" Steel Rod, Threshold Crossing, 5,145.6 m/s (Standardized)

The revised velocity still shows a slight degree of skewness to greater than 0.05 meter distance, caused by the greater quantity of good samples in the long distance test. The majority of results of the resolution tests are now within 0.002 meter (2 mm) of the

measured distance. Using this better approximation of the wave velocity, the Digital Wave Fracture Wave Detector is capable of consistently determining an accurate source location in the homogeneous, thin (1/8" diameter) rod sample.

C. MEASUREMENT OF DISPERSION

As noted in the investigation of the 3/8" rod, dispersion of the signal was a concern. If the wave speed changes in the length of the bar, resolution and accuracy will change based on what lineal position in the bar the measurement is taken at. Changes in wave speed would be mainly due to higher frequencies (and accompanying higher velocities) not being transmitted the entire length of the bar. To quantify the effects of dispersion, a 0.050 meter (50 mm) distance was measured using the same methodology as above. However, this same gauge distance was measured at different distances from the acoustic source, termed "far", "intermediate", and "near". This configuration is shown in Figure 5.8, below.

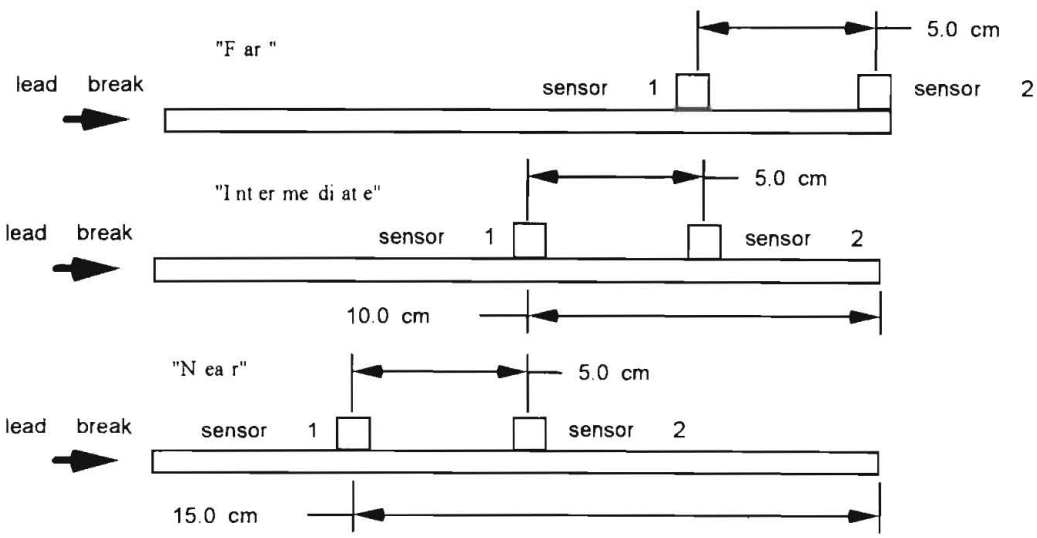

Figure 5.8, Dispersion Tests

Comparison of the measurement using an appropriate (and consistent) velocity will show the effect of dispersion of the higher frequencies on the waveform throughout the rod. In a manner similiar to the resolution tests, a Microsoft Excel spreadsheet was used to categorize measured distances into a histogram. In this series of tests, all the measurements were 0.05meter, so no standardization of the data was necessary. In the case of the 3/8" rod, 5300 m/s was used as the wave speed. This was only for consistency with the previous resolution series of experiments.

Results for the 3/8" rod are presented in Figure 5.9, below.

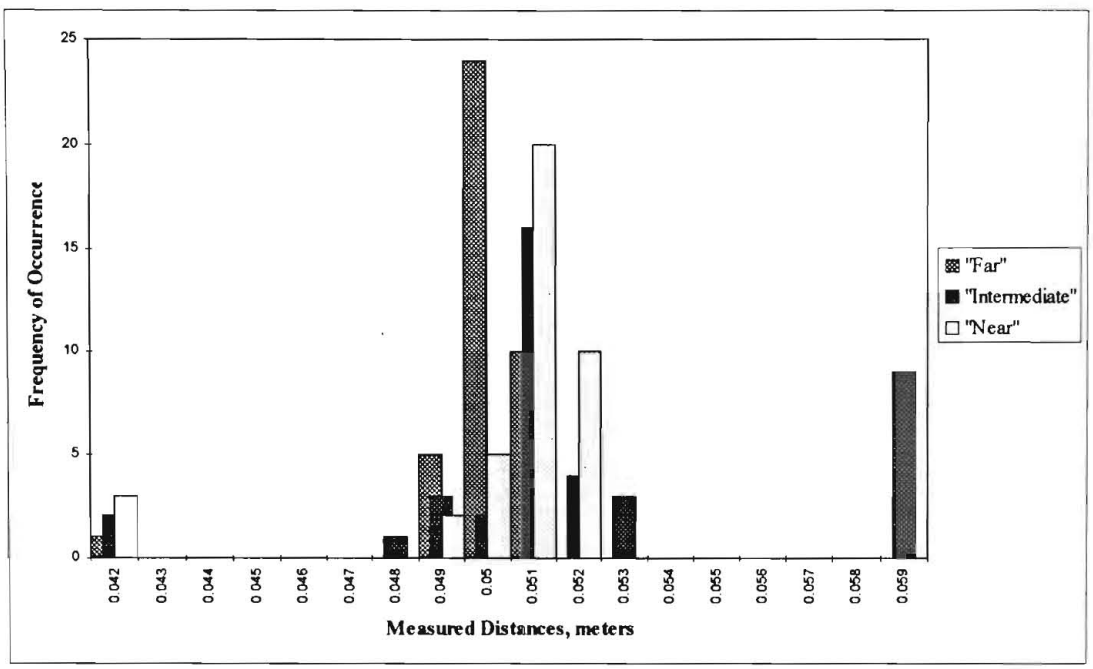

Figure 5.9, 3/8" Steel Rod, Threshold Crossing, 5,300 m/s

It can be seen from the histogram in Figure 5.9 that the central tendency of the measured distance is slightly greater than actual separation of 0.05 meter. Important to note, however, is the large variability in the different measuring points from the known

distance of 0.05 meter. The near measurements err on the positive side by approximately 0.0015 meter (1.5 mm). The far measurements err on the negative side by the same margin. This shows that the initial arrival wave's frequency (and hence wave velocity) is different at the 3 different sets of measurements. The high frequency components of the extensional wave are known to be dispersive. This is consistent with the difficulty noted in the distance resolution tests on the 3/8" rod.

The histogram for the 1/8" steel rod is presented in Figure 5.10.

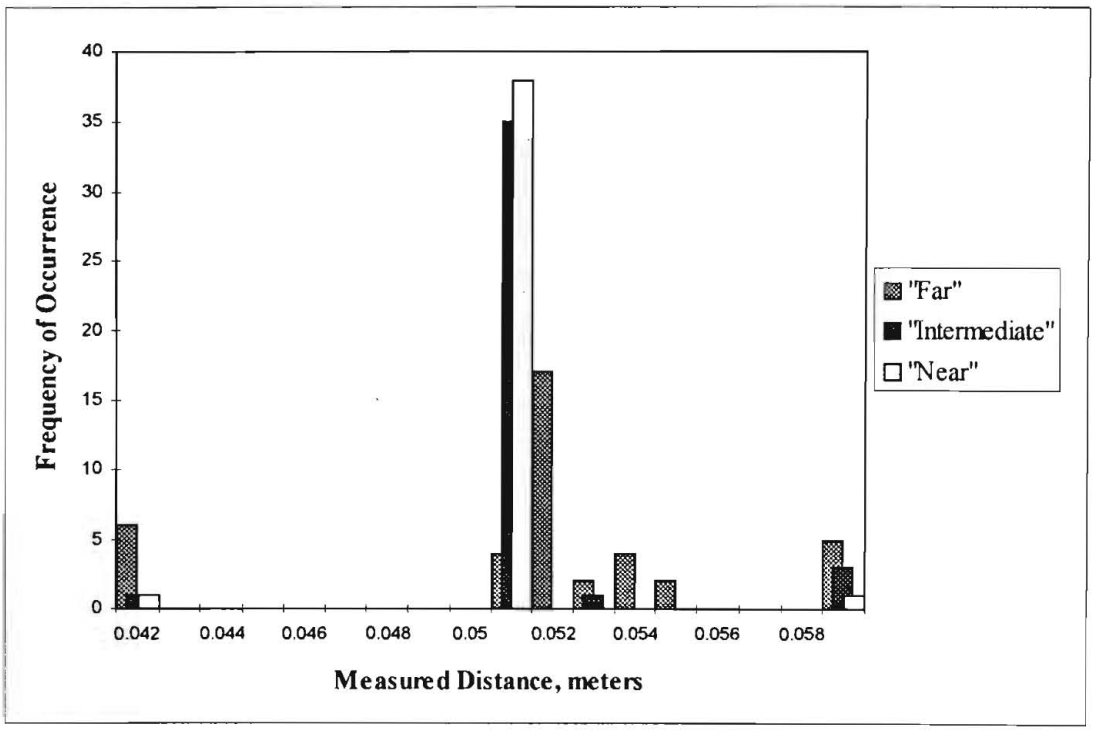

Figure 5.10, 1/8" Steel Rod, Threshold Crossing, 5,300 m/s

As Figure 5.10 was plotted using 5300 meters / second as the wave velocity, the central tendency is again skewed to approximately 0.0515 meter. Operating the threshold

crossing routine on the data a second time with the revised velocity of 5146 meters / second produces the histogram shown in Figure 5.11.

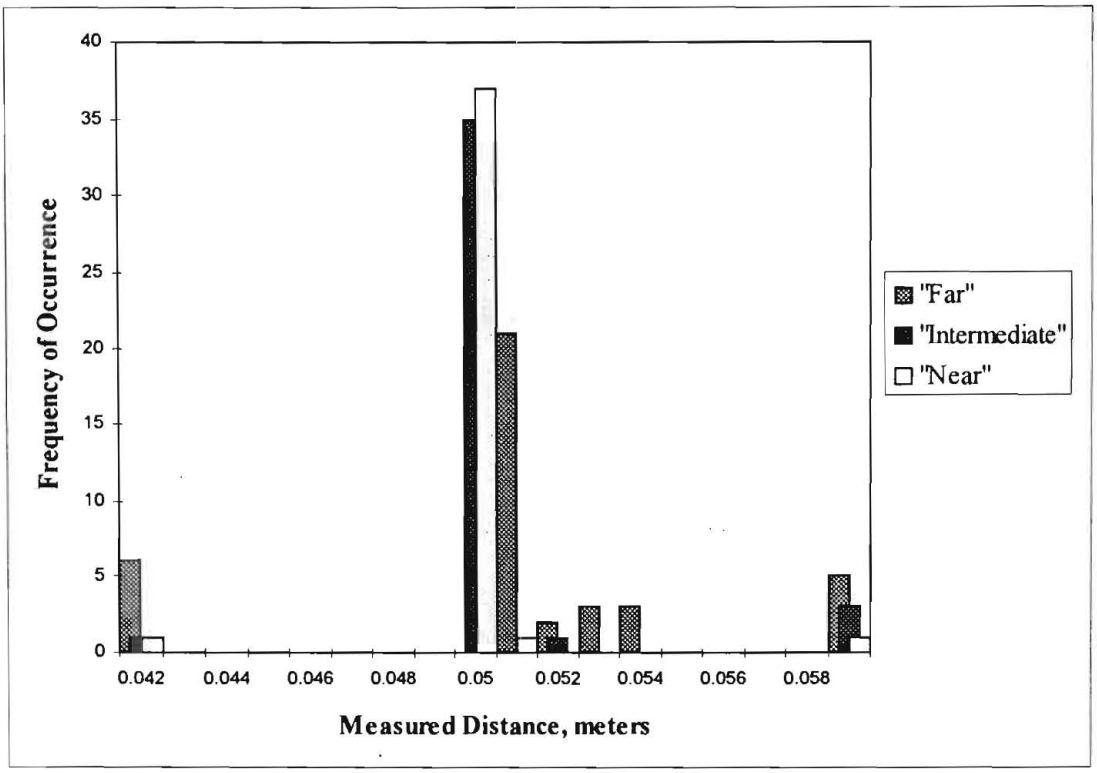

Figure 5.11, 1/8" Steel Rod, Threshold Crossing, 5,145.6 m/s

The mean measured distance is now nearly exactly 0.050 meter in the near and middle measurements. The measurements at the far end of the bar still display some error, possibly due to dispersion effects beginning to become signifigant.

Common to both the resolution and dispersion tests is the greater variability in the results of the 3/8" bar. Again comparing the waveforms displayed in Figure 5.6, it can be noted that the arrival wave in both cases is of high frequency and extensional in character. In the 1/8" rod it appears to be of a more singular frequency. The 3/8" rod's arrival wave is also of high frequency, but appears to contain several higher order modes. These modes

considered to be variations from the ideal behavior of a thin rod. As the relationship between wavelength and diameter of the waveguide increases, the correlation with classical rod theory deteriorates. The character of the waveguide begins to more closely follow those of bulk materials. As the thin rod gives satisfactory results, the discussion of bulk properties will not be considered.

As an intermediate step in the investigation of composite materials, these results are an adequate presentation of acoustic emission techniques in isotropic materials. Using the revised velocity of 5145.6 meters / second, the Digital Wave system is capable of measuring distances in thin (1/8' diameter) homogeneous steel rods with acceptable accuracy.

VI. RESULTS OF SOURCE LOCATION IN COMPOSITE MATERIALS

A. EXPERIMENTAL METHOD

The method used to determine the ability of the software to accurately measure distances in unidirectional composite strands is nearly identical to the method used for the isotropic steel rods (Section IV). The location and identification of sensors were identical. In addition to the threshold crossing method of time determination, the Gaussian cross correlation method was shown to be effective in the composite strand. The carbon fiber composite strand required significantly greater amplification of the wave signal to trigger and record data. This increased the amount of noise recorded with the signal. This noise was on the order of a level of approximately 0.1 volt, necessitating a threshold of 0.2 volts to accurately measure the initial wave. In the following discussion, the Gaussian cross correlation algorithim was demonstrated to greatly increase the accuracy of the measured distance.

B. RESOLUTION OF SOURCE LOCATION

The first experiments to quantify the spatial resolution of a stress wave source on the composite strand were similiar to those used in the experiments on the isotropic steel rod. The carbon fiber composite strand was 140 mm long, measured between the mounting tabs. For the distance resolution experiments, three distances were measured, 0.140, 0.070 and 0.035 meters (140, 70 and 35 mm). The configuration of the test sensors is shown in Figure 6.1.

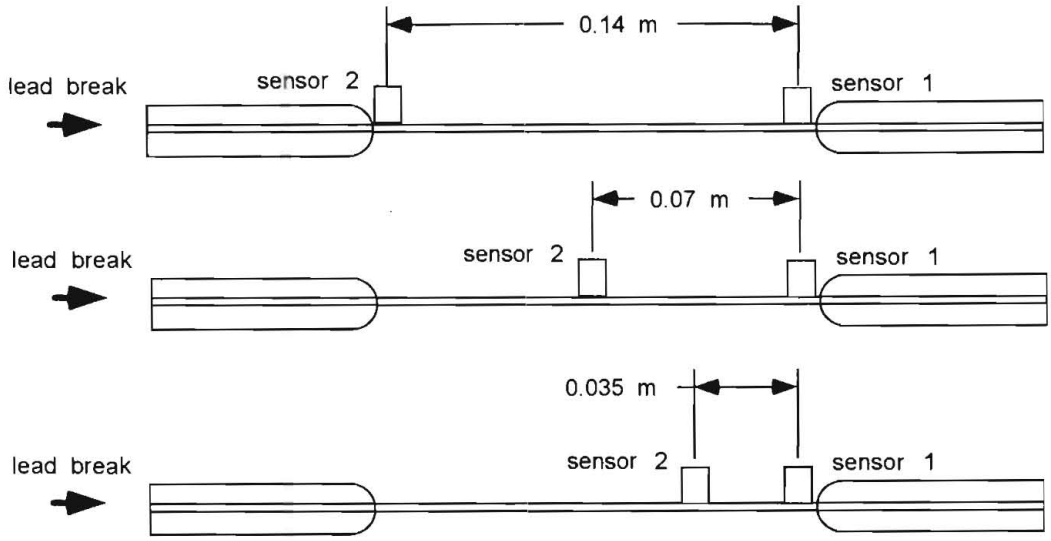

Figure 6.1, Distance Resolution Test, Carbon Fiber Sample

Each test configuration was subjected to 50 lead break events using the same pencil lead as previously described. The carbon fiber / epoxy matrix strand was found to attenuate the signal produced by the lead break rather signifigantly. Total amplification of 76 dB (preamplifiers and main unit total) was required as compared to 36 dB (approximate average) used in the isotropic cases. This high degree of amplification also greatly increased the noise present in the wave form as seen in Figure 6.2. (compare to Figure 5.6)

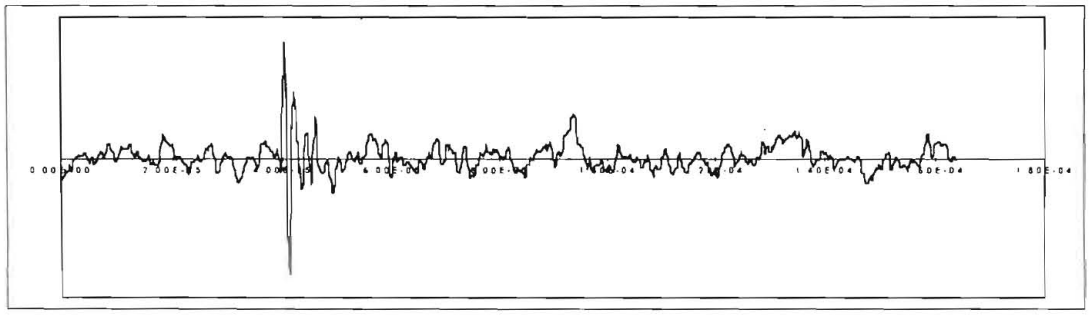

Figure 6.2, Example Waveform in Carbon Fiber, Measured at Center of Strand

This high level of noise necessitated an increase in the threshold level by an order of magnitude compared to the isotropic samples. The threshold level used was 0.2 volt, compared to 0.02 volt in the isotropic case. The extensional mode is still sharply defined, even when compared at this higher voltage level. Wave propagation speed of 10,000 meters / second was estimated using values provided by Hercules product data(1991) for modulus and density of the carbon fiber material. Figure 6.3 is a histogram of the 50 repititions for each of the 3 spatial seperations using the threshold crossing technique with a threshold of 0.2 volt and a wave speed of 10,000 meters / second.

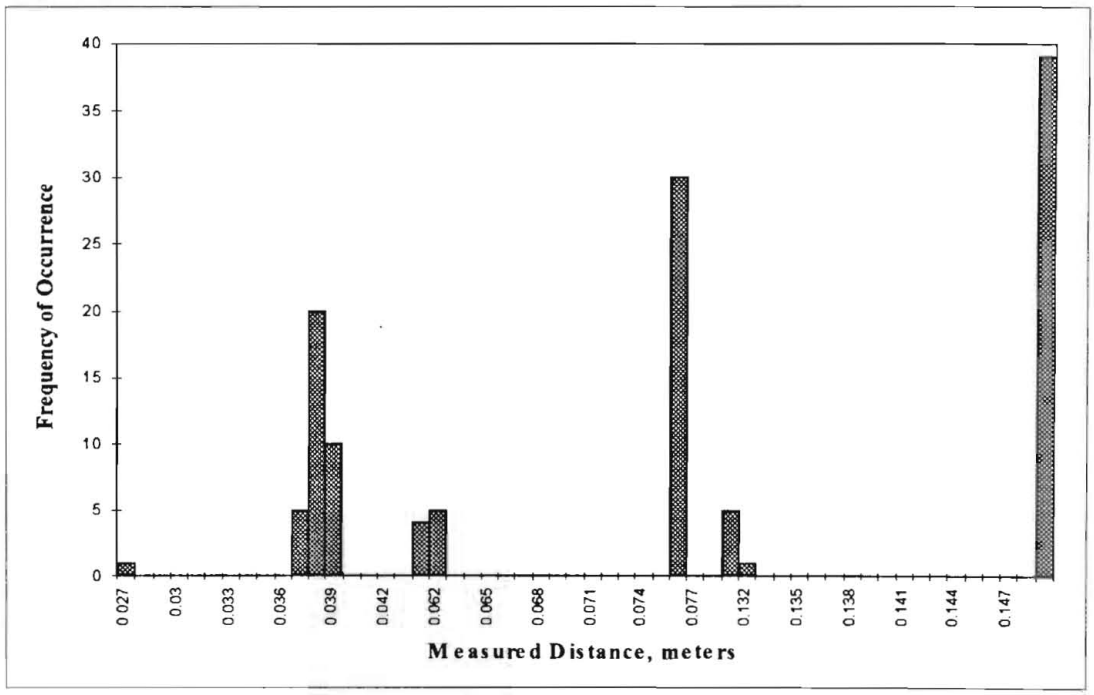

Figure 6.3, Carbon Fiber Distance Resolution, 10,000 m/s

This same data is displayed standardized to the known 0.035 meter distance by the previously described axis shift in Figure 6.4. It can be readily seen that the threshold crossing technique is in error.

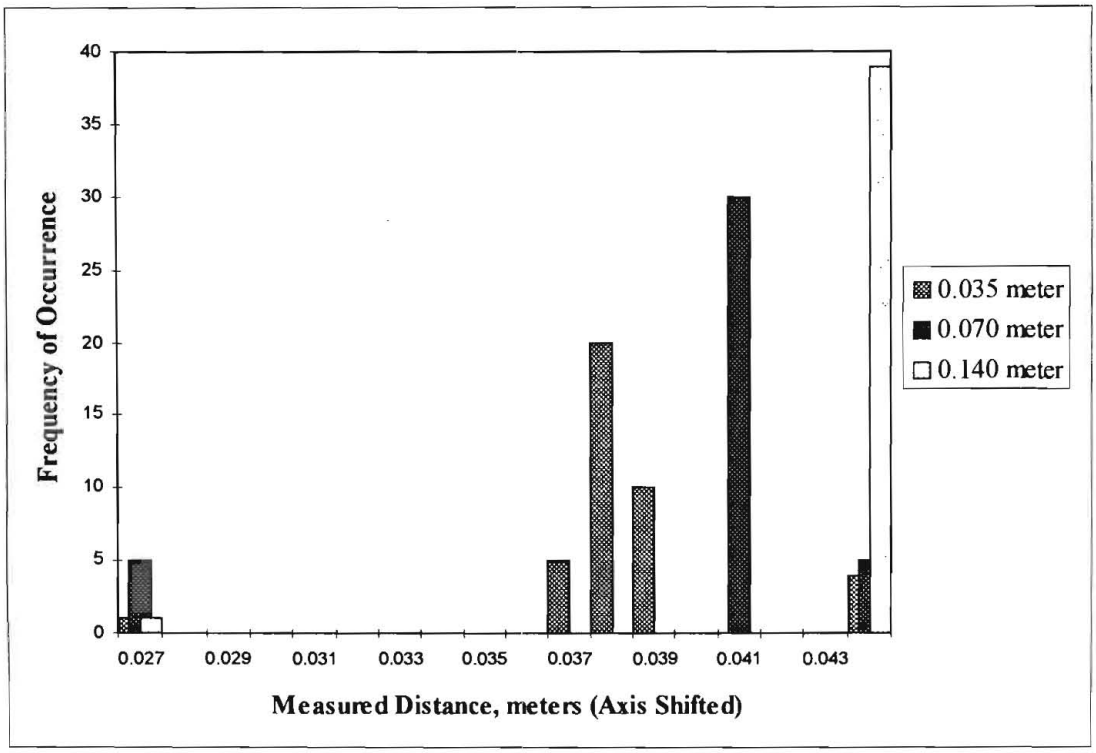

Figure 6.4, Carbon Fiber Distance Resolution 10,000 m/s (Standardized)

All the data points are skewed to the long side and in error by betewen 0.003 and 0.010 meters. The distribution is not formed well enough to even obtain a meaningful mean value. As the error is dependent on length of the distance measured, dispersion of the high frequency components of the wave is a possible explanation.

As all the data in the previous series were skewed to the long side, we investigate the possibility of compensation by adjusting the wave propogation speed in the threshold crossing algorithim. Figure 6.5 and 6.6 display threshold crossing data for the same samples analyzed with the previous 0.2 volt threshold and a revised velocity of 8,700 m/s vs the originally computed 10,000 m/s .

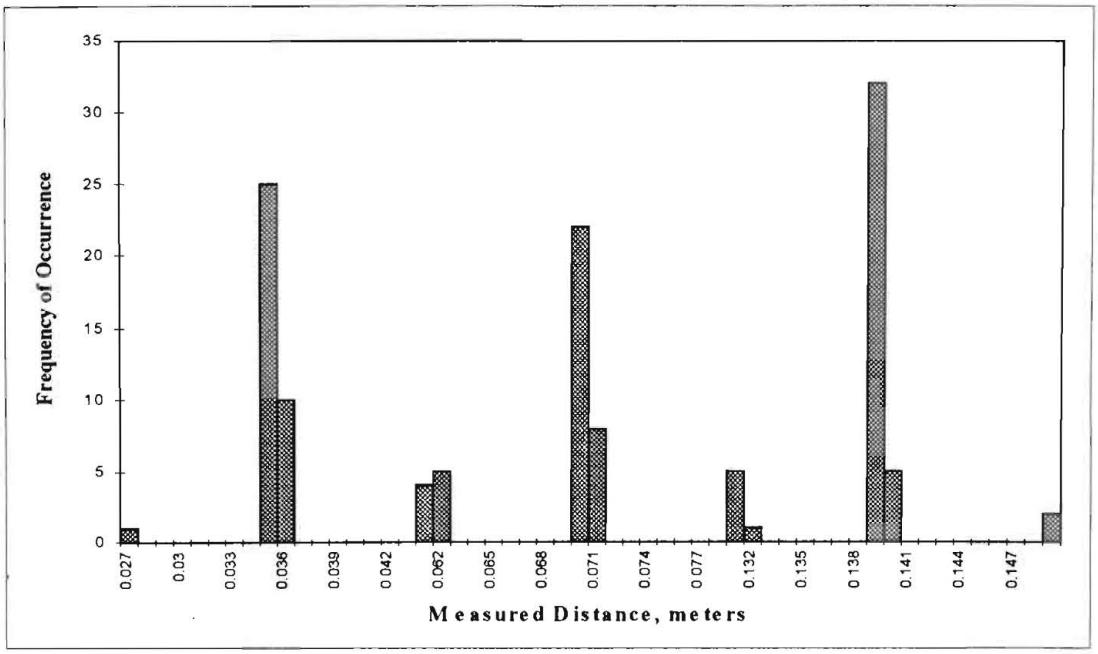

Figure 6.5, Carbon Fiber Threshold Crossing, 8,700 m/s

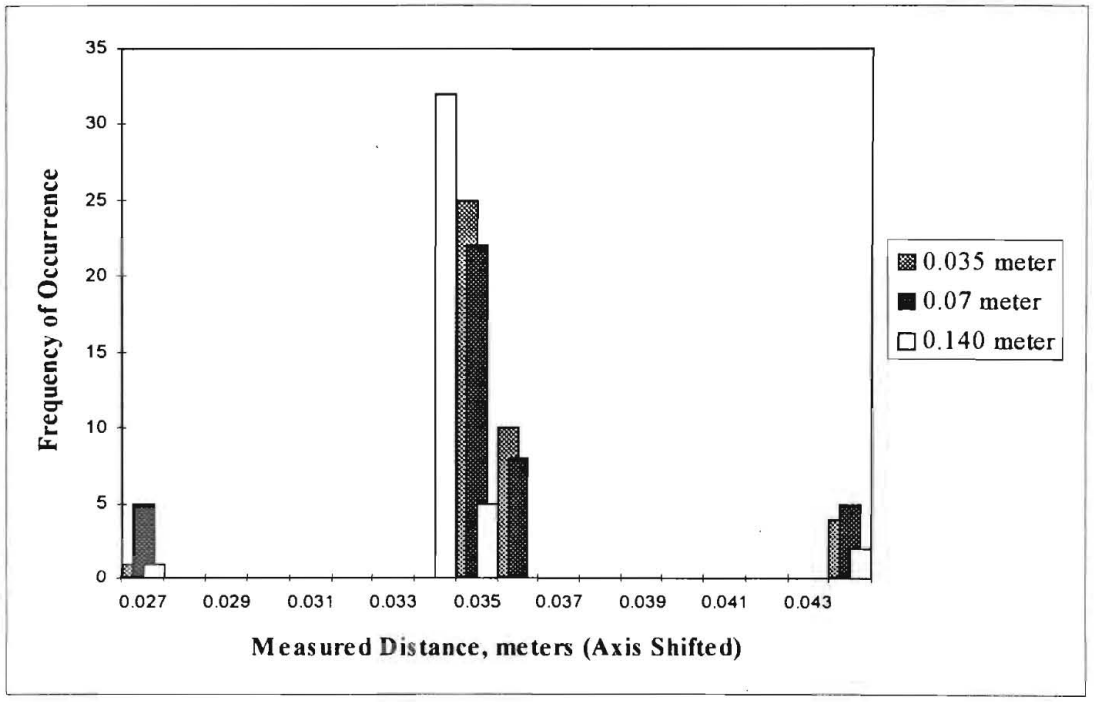

Figure 6.6, Carbon Fiber, Threshold Crossing 8,700 m/s (Standardized)

It can be observed from Figure 6.6 that the central tendency of correct distance measurement can be compensated for by use of an effective velocity. The skewing and dispersion of the measurement, though reduced is still present. The greater dispersion seen in Figure 6.4 (compared to Figure 6.6) is most likely caused by the higher velocity accentuating differences in the elapsed time. That is, at higher velocitys small variations in time produce more pronounced variation in distance since the total time involved is signifigantly less.

C. MEASUREMENT OF DISPERSION

Although the differences in distances measured by the threshold crossing alogorithim in the previous section could be compensated for by optimizing the wave velocity, a more accurate test of dispersion was required to reduce the measurement's dependence on distance. The tests follow the configuration used in the isotropic example. That is, a constant distance is measured at three different distances from the acoustic event. In the case of the carbon fiber sample, 0.035 meter (35 mm) was chosen as the representative distance. It was measured at three points, as shown in Figure 6.7, below. Again, the three configurations are refered to as "Far", "Intermediate", and "Near."

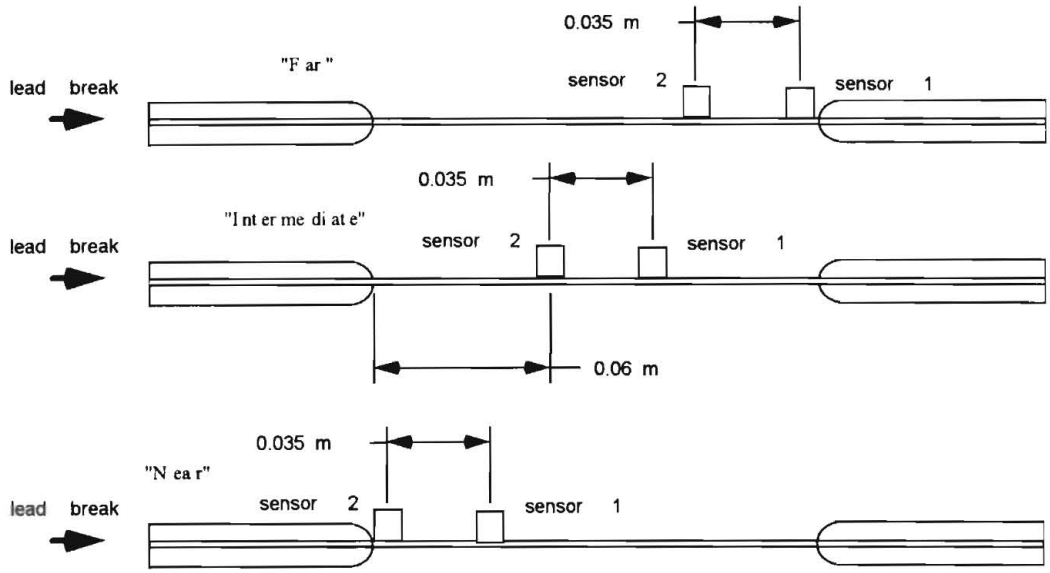

Figure 6.7, Dispersion Test Configuration, Carbon Fiber Sample

Again, 50 lead breaks were used for each test. Figure 6.8 shows results of the dispersion tests, computed using the previously determined threshold crossing parameters of 8,700 meters / second and a voltage threshold of 0.2 volts.

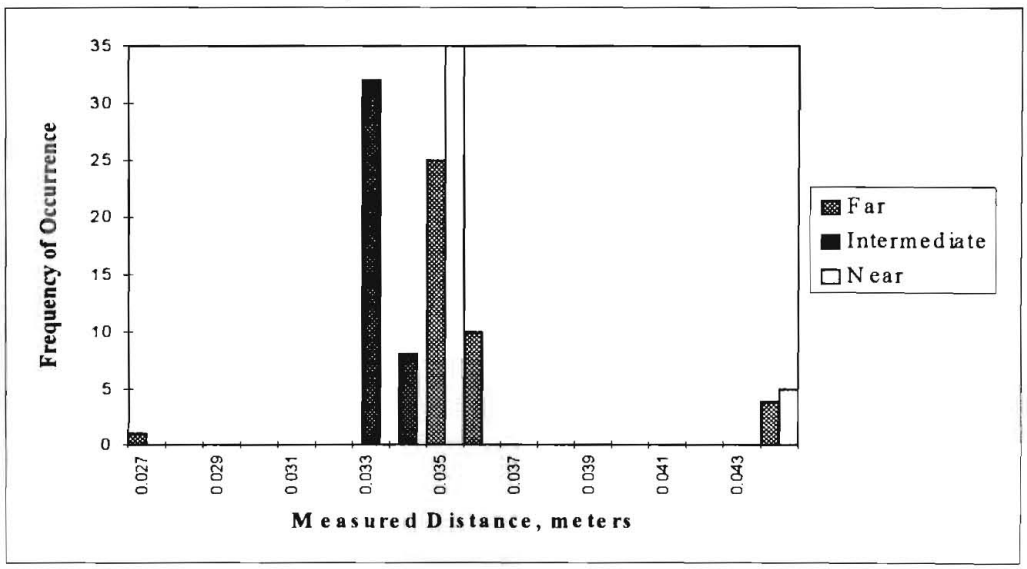

Figure 6.8, Carbon Fiber, 8,700 m/s

Figure 6.8 shows that the central tendency of the measurement accuracy is consistent with the resolution of 0.003 m. Two discrepancies still need to be addressed. They are: 1) there exists some extreme outlying measurements, and 2) the order of the error in the intermediate, near and far measurements are inconsistent with the physical expectations of the dispersion phenomenon. That is, given dispersion increasing with the distance from the source, the order of accuracy should be near, intermediate, and far, instead of intermingled (far is between intermediate and near).

In an attempt to correct this discrepancy, the Gaussian cross correlation technique of the Digital Wave software was used to analyze the dispersion data. A two parameter analysis was undertaken to determine the best frequency and wave propogation speed to use in the cross correlation technique (Appendix B). The results of the Gaussian cross correlation at 700 kHz and a wave propagation velocity of 8,700 m/s are presented in Figure 6.9.

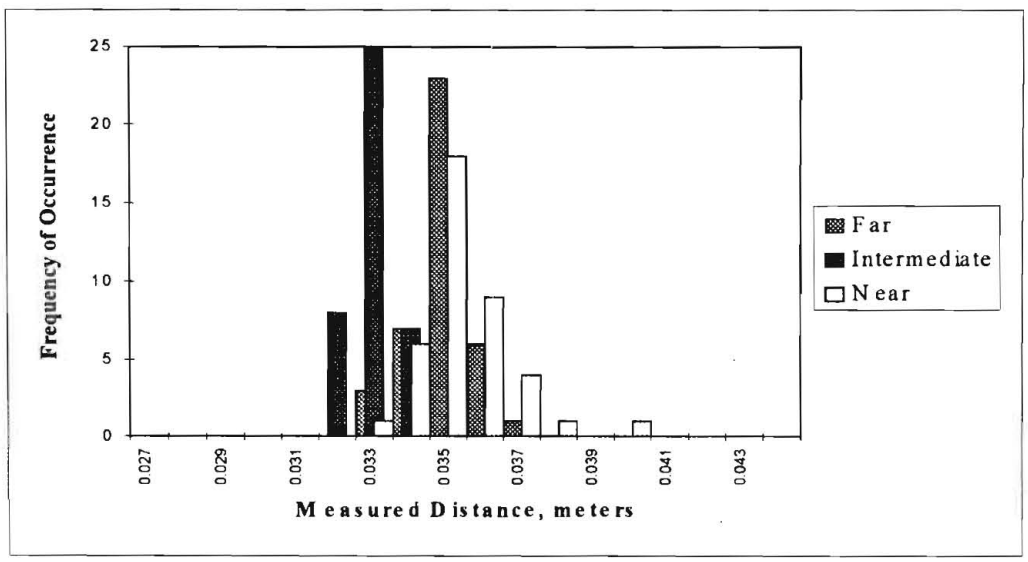

Figure 6.9, Gaussian Cross Correlation 8,700 m/s @ 700 kHz

The data from the intermediate configuration is still skewed to the short side, but all measurements are normally distributed about the expected value of 0.035 m. Additionally, extreme outlying values were eliminated. It is also noted that for the majority of measurements the accuracy and the resolution are now brought to be the same value of 0.003 meters (3 mm).

The extensional wave is the primary arrival wave in the carbon fiber strand. The dispersion present in this extensional wave created anomalies when using threshold crossing as a means of source location. High attenuation of the signal caused by the matrix binder neccesitates high amplification levels and associated noise. The resultant noise floor requires a higher threshold voltage setting than previously encountered, but still produce adequate results. At the amplitude level of the signal used in the experimentation, the magnitude of error does not prohibit the use of threshold crossing as a means of source location.

Gaussian cross correlation was capable of correcting some anomalies present in the data interpreted with threshold crossing. More importantly, the accuracy is made to coincide with the maximum resolution available in the sensors. Gaussian cross correlation is the recommended algorithim of choice.

VII. CONCLUSIONS

This investigation explores the use of acoustic emission measurements to locate the source of internal damages (fiber breaks) in a composite. Specifically, the resolution and accuracy of the Fracture Wave Detector model F4000, a state of the art acoustic emission system produced by the Digital Wave Corporation, were quantified. The dependency of resolution and accuracy on attenuation and dispersion were also characterized.

For definitiveness, source locations in one dimensional rods were investigated. Benchmark tests were performed on homogeneous, isotropic steel round rods chosen for the material's relatively low dispersion and attenuation properties. Unidirectional graphite fiber in an epoxy matrix was used to characterize the wave propagation effects due to heterogeneity, micro-wave guide, and a highly attenuative matrix. To determine the difference in arrival times of the waveforms, two algorithms were compared; one, based on simple threshold crossing, the other based on cross-correlation with a Gaussian, amplitude modulated wave at a target frequency.

Because the ultimate goal is to measure internal damages, the stress wave source is expected to be dominated by extensional waves which lend themselves to transducer placement perpendicular to the wave front, i.e. the end of the rod. The experimentally expedient location for transducer mounting is on the side of the rod. These two mounting locations are compared. Based on the transducer mounting perpendicular to the extensional wave, the side mounted transducer's (sensor surface parallel to the wave

direction) resolution was determined to be 0.003 meters. Because of the steel's low attenuation only a moderate amount of amplification is required. The extensional wave's low dispersion in the isotropic medium makes the simple threshold crossing algorithm adequate for both accuracy and repeatability.

The measurements on the composite sample were complicated by the material's high attenuation which necessitated high signal amplification. This in turn leads to amplification of background noise to a signifigant level. The high noise level necessitated moving the threshold voltage to a level 10 times higher than that used in the steel rod. The higher wave speed associated with the carbon fiber made the threshold crossing algorithim more sensitive to small errors caused by dispersion in the carbon fiber strand. The dispersion also resulted in measurement resolution errors greater than the accuracy of the sensors. Digital Wave's Gaussian cross correlation algorithm was found to be capable of accurately determining the source location within the previously determined resolution (0.003 meter) of the sensor. The Gaussian correlation algorithm is the recommended method for source location in composite using surface mounted transducers; even for primarily extensional waves.

For repeatability, the stress wave source used in the measurements conducted herein were generated from a abrupt lead beak. The relative magnitude of these artificial events compared to the actual fiber rupture events are not known. The extension of the conclusions presented herein awaits the confirmation of detection of actual fiber breakage of composite due to applied tensile loads.

APPENDIX A. MATERIALS AND EQUIPMENT

All measurements of acoustic emissions were carried out using the Digital Wave Corporation's Fracture Wave Detector model F4000. Complete operating instructions including theory of use are available in the operating manual and will not be discussed further. Specific procedures concerning data collection in rod samples will be covered in detail.

Two samples of hardened steel rod were prepared by machining the ends perpendicular in a lathe and marking the center of the diameters with a center punch. The samples were: 1) 3/8" in diameter by 0.206 meter (206 mm) in length, and 2) 1/8" in diameter by 0.212 meter (212 mm) in length. The length measurements are reported in metric units to be consistent with the units used in the Digital Wave software. Differences in length were not considered important as only measured portions of the rods were used in experiments.

A single sample of AS-4 carbon fiber strand was taken from a lot of 60 samples provided by the Hercules Corporation. The composite strands are manufactured by encapsulating a 12,000 filament bundle in an expoxy (Dow DER 323) matrix. The ends of the sample were encased in a tab of plastic resin approximately 0.055 meter (55mm) long to facilitate gripping in a tensile test machine Overall length of the sample was approximately 0.260 meter (260 mm). The length of the composite strand was approximately 0.245 meter (245 mm). Approximately 0.005 meter (5 mm) of the resin tab

was removed using a water cooled diamond saw to expose the end face of the actual carbon fiber strand.

The Digital Wave system consists of the F4000 signal processor, a Compaq brand 486 personal computer, two preamplifiers and two transducers. The basic layout of the system is shown in Figure A.1. The computer and signal processor are connected by a ribbon cable and proprietary analog / digital conversion card. The preamplifiers are connected to the signal processor by two cables, one for signal transmission and the other to provide power to the preamplifiers from dedicated power supplies in the signal processor. The transducers are connected by lengths of 55 ohm coaxial cable.

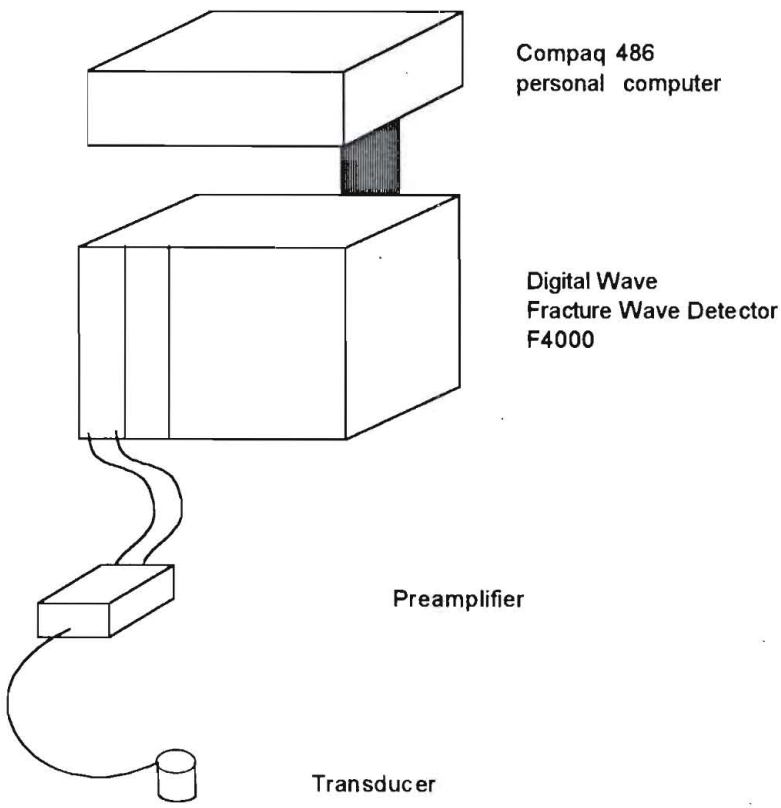

Figure A.1, Basic Componetry and Layout of Acoustic Emission Equipment

Throughout the testing conducted, preamplifiers and transducers were dedicated to specific channels of the signal processor and were not varied. Serial numbers are provided in table A.1. Initial testing showed a defect in the channel 2 transducer. This was replaced with the transducer indicated below. Calibration data from two transducers (conducted by Digital Wave) show them to be nearly identical.

	Preamplifier	Transducer
	Serial number	Serial Number
Channel 1	036	951293
Channel 2	045	945020

Table A.1, Equipment Data

All lead breaks were executed using a mechanical lead pencil containing Pentel brand 0.3 mm (0.0012") 2H lead. All leads were from one gross lot purchased as a unit. For the most part, Dow Corning Silicone Vacuum grease was used as an acoustic couplant between the rod samples and the transducers. Dow Corning number 33, Extreme Low Temp Bearing Grease, Medium Consistency was also utilized. Although nearly identical in acoustic transmission, the vacuum grease was found to provide better adhesion between the transducers and the rod, especially in the thin rod case.

APPENDIX B. - TWO PARAMETER ANALYSIS OF CROSS CORRELATION

Use of the Digital Wave Gaussian Cross Correlation algorithm to measure distances in carbon fiber strands requires optimization of two user input variable parameters to obtain the best results. As discussed in Chapter V, the threshold crossing algorithim initially provided accurate measurement in isotropic steel bars. When this threshold method was applied to the measurements of the carbon fiber composite, anomalies are caused by the higher attenuative and dispersive properties of the matrix. The initial wave propagation velocity of 10,000 m/s skewed location data approximately 8%. Correcting wave propagation speed to 8,700 meters / second corrected distance resolution, but results of dispersion tests were not consistent. Since both wave propagation speed and cross correlation frequency are selected by the user, the following series of experiments were performed to optimize these parameters.

The Digital Wave software returns the difference in arrival times measured in addition to its computation of the location. With the threshold crossing algorithim, this is determined by difference in times that the signal from the two channels crosses the same set threshold voltage. In the Gaussian cross correlation technique, it is the difference in time between the best correlation of the signal from each channel with a Gaussian modulated (amplitude) pulse of a set frequency.

To determine the frequency to be used for the cross correlation, arrival waves were measured for principle frequency. Initial measurement of the arrival wave indicated an approximate frequency of 750 kHz. For accurate measurement and correlation, the

frequency component must be present in both arrival waves. Using the 750 kHz measurement as a reference, iteration at 50 kHz intervals was used between 600 kHz and 800 kHz. As dispersion effects are most pronounced in the higher frequencies, the range of tested frequencies was skewed to lower than the representative frequency.

Wave propagation speed is also a user input variable in the Digital Wave software. As 8,700 meters / second gave good results when used with threshold crossing in the initial resolution survey, this was the speed used as a reference in this investigation.

In all five data sets were analyzed using different correlation frequencies. They are the three distance resolution tests depicted in Figure 6.2 and the three dispersion tests depicted in Figure 6.7. The third resolution test corresponds to the first dispersion test and is not repeated, resulting in five data sets. The 0.140 meter and 0.070 meter distances were normalized to 0.035 meter to more clearly show variances.

Each set of these normalized arrival times was tabulated to compute the mean and standard deviation. The best case would be a cross correlation frequency that returns the same mean arrival time difference with a small standard deviation. Mean and standard deviation data is presented in Table B.1 and Table B.2

Cross Correlation Frequency (kHz)	0.140 m	0.070 m	0.035 m	0.035 m, intermediate	0.035 m, far
600	3.8568E-06	4.5568E-06	3.4016E-06	3.4432E-06	3.9904E-06
650	4.156E-06	4.1232E-06	3.8688E-06	3.5232E-06	4.2144E-06
700	4.1272E-06	4.0368E-06	3.8592E-06	3.7824E-06	3.786E-06
750	4.5864E-06	3.9856E-06	3.696E-06	3.4912E-06	3.8176E-06
800	4.9352E-06	4.2352E-06	3.5712E-06	3.5712E-06	3.8112E-06

Table B.1, Mean Arrival Times, milliseconds

Cross Corellation Frequency,(kHz)	140 mm	70 mm	35 mm	35 mm, middle	35 mm, far
600	2.22913E-06	4.77923E-06	1.888E-07	1.54265E-07	2.18001E-07
650	2.4985E-06	1.33427E-06	1.85738E-07	1.95933E-07	2.03923E-07
700	2.51887E-06	1.23316E-06	1.91038E-07	5.73113E-07	5.73021E-07
750	4.56172E-06	1.19505E-06	2.22279E-07	1.45556E-07	3.50558E-07
800	6.30344E-06	2.80203E-06	3.14252E-07	1.44674E-07	3.60182E-07

Table B.2, Standard Deviation of Arrival Times, milliseconds

The data from Table B.1 is presented graphically in Figure B.1. It is obvious from Figure B.1 that correlation at 700 kHz gives the most stable mean value. Since this information is raw time data, actual distance can be easily adjusted by changing the previously fixed velocity of 8,700 meters / second.

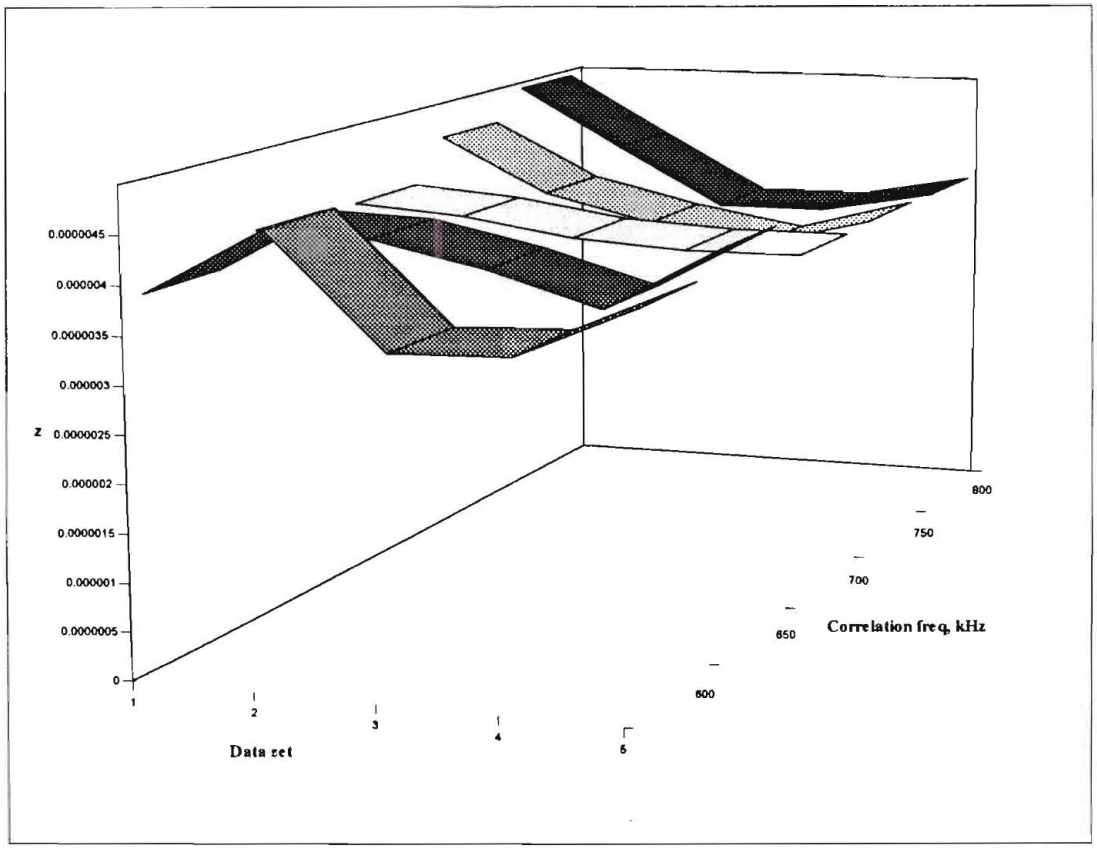

Figure B.1, Mean Arrival Time Differences

Standard deviation data is presented graphically in Figure B.2, below. It can be seen that the fit is not as good when measured over long distances (0.14 meter and 0.07 meter). It can still be seen that a correlation frequency of 700 kHz appeared to be most efficient to minimize the standard deviation over the broadest range of distance measurements. It is noted that the standard deviations presented are artificially low as an artifact of the normalization. When not normalized the standard deviation in the 0.07 meter and 0.14 meter samples are greater, on the order of 0.01 m (0.07 meter sample) and 0.04 m (0.14 meter sample) when converted to distances.

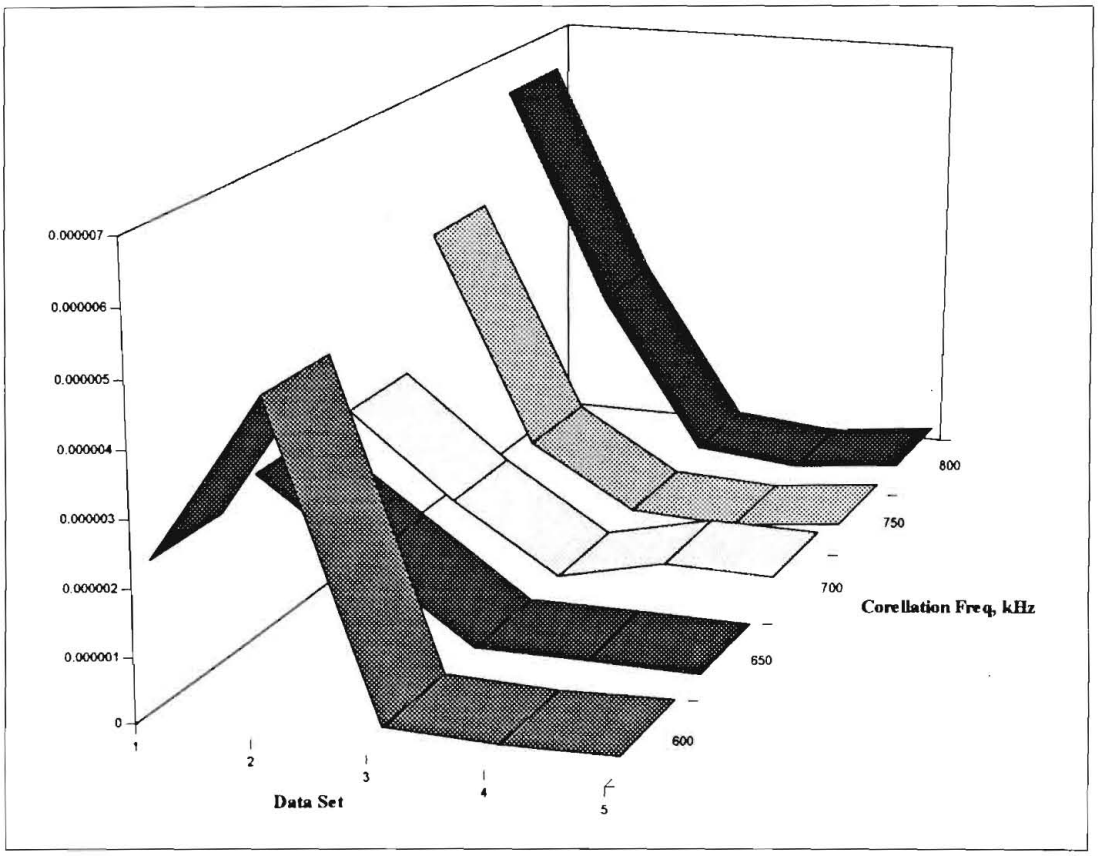

Figure B.2, Standard Deviation

Actual distance information from the cross correlation at 700 kHz and 8,700 meters / second was plotted using the same Excel spreadsheet described in Chapter V. Using these determined Gaussian cross correlation parameters, the results of the distance resolution test shown in Figure 6.1 are presented in Figure B.3. The data is presented in the previously described standardized format, corrected to 0.035 m.

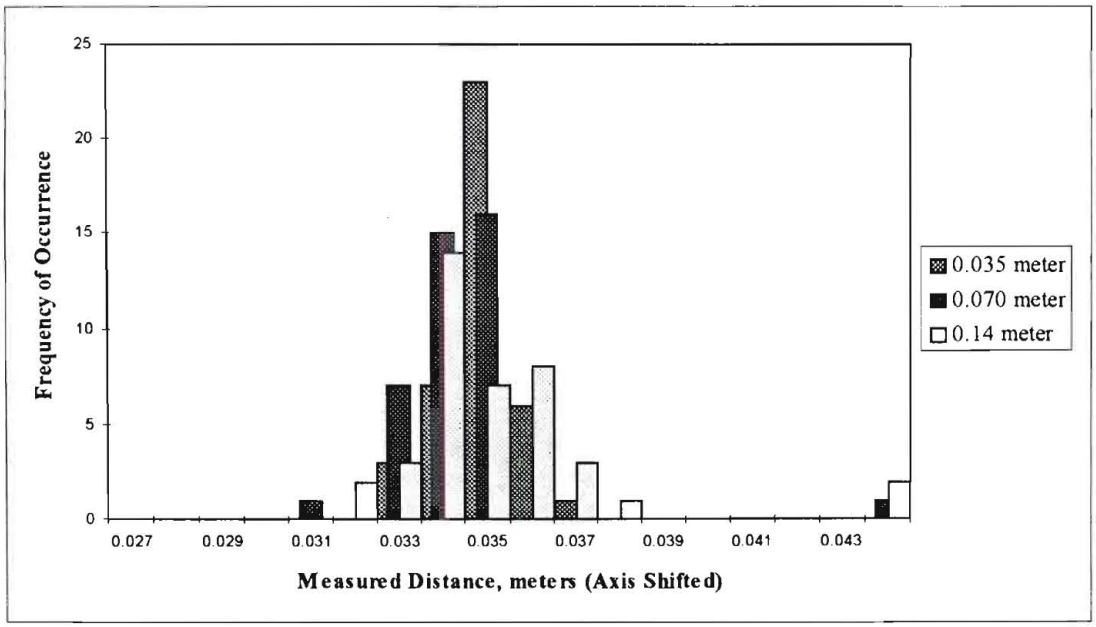

Figure B.3, Carbon Fiber, Gauss Cross Correlation @700 kHz, 8,700 m/s (Standardized)

For comparison, the threshold crossing results from the same test configuration (Figure 6.6) are repeated in Figure B.4

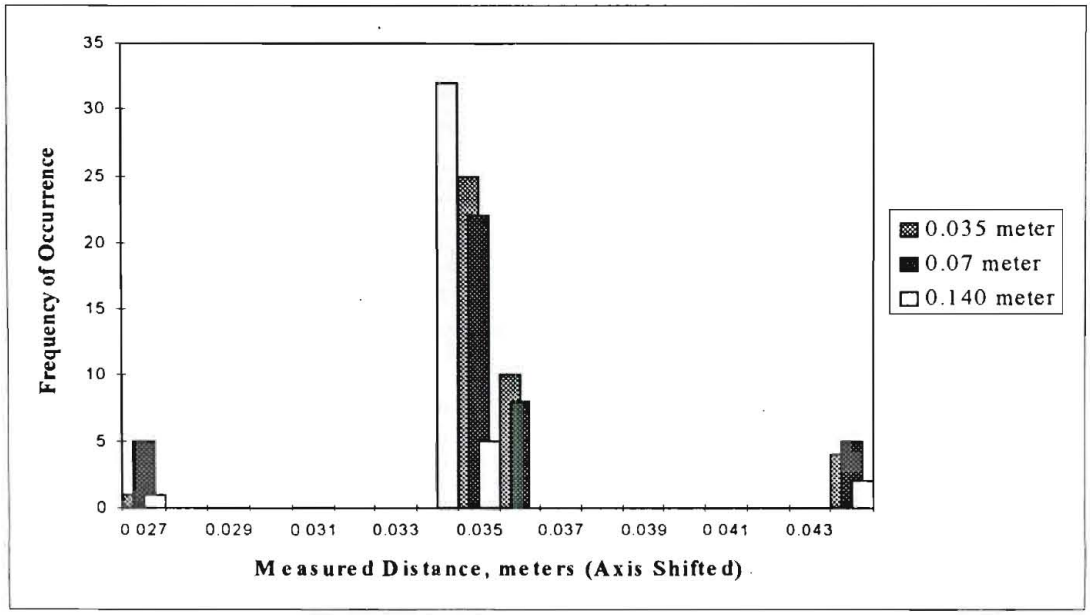

Figure B.4, Carbon Fiber, Threshold Crossing, 8,700 meters / second, (Standardized)

It can be seen that the apparent mean of the measured distances are both coincident at 0.035 meter. The Gaussian cross correlation provides a greater deviation about the mean, but is still accurate within 3 mm in all cases.

Figure B.3 indicates that the optimizing the carrier velocity and the correlation frequency corrects the inconsistent ordering of accuracies between the near, intermediate, and far data sets. This is accomplished while preserving the accuracy and resolution of the sensors.

LIST OF REFERENCES

Chamis, C. C., "Micromechanics Strength Theories,"*Composite Materials*, vol 5, Academic Press,1974.

Digital Wave Corporation, Fracture Wave Detector, Instruction Manual

Gorman, M. R., and Ziola, S. M., "Plate Waves Produced by Transverse Matrix Cracking," *Ultrasonics*, v. 29, n. 3, pp. 245-251, May 1991

Graff, Karl F., *Wave Motion in Elastic Solids*, Dover Publications, Inc., 1991.

Harlow, D. G., and Phoenix, S. L., "Probability Distribution for the Strength of Composite Materials I and II", *Int. Journal of Fracture*, v. 17, pp 372-437 and 601-630, 1981

Hercules Product data sheet, AS-4 fiber, number 847-6, August 1991.

Hercules Product data sheet, AS-4C fiber, number 876-1, August 1991.

Hsu, N. N., and Hardy, S. C., "Experiments In Acoustic Emission Waveform Analysis for Characterization of AE Sources, Sensors and Structures," *Elastic Waves and Non-Destructive Testing of Materials*, Applied Mechanics Division, v. 29, pp. 85-106, December 1978.

Kolsky, H., *Stress Waves in Solids*, Dover Publications, Inc., 1963.

Pao, Y, H., "Theory of Acoustic Emission," *Elastic Waves and Non-Destructive Testing of Materials*, Applied Mechanics Division, v. 29, pp 107-128., December 1978

Sachse,W., Netravali, A. N., and Baker, A. R., "An Enhanced, Acoustic Emission - Based, Single - Fiber Composite Test," *Journal of Nondestructive Evaluation*, Vol 11, Nos. 3/4, 1992.

Wu, Edward M. and Bell, David K., "Proof Test Methodology for Composites," *Proc. Ninth DoD/NASA/FAA Conf. on Fibrous Composites in Structural Design*, v. 2, pp 549-560, September 1992.

Ziola, Steven M., "Source Location in Thin Plates Using Crosscorrelation," Monterey, CA, 1991.

INITIAL DISTRIBUTION LIST

1. Defense Technical Information Center 2
   Cameron Station
   Alexandria, Virginia 22304-6145

2. Library, Code 52 2
   Naval Postgraduate School
   Monterey, California 93943-5101

3. Digital Wave Corporation 2
   14 Inverness Drive East
   Building B, Suite 120
   Englewood, Colorado 80112
   Attn : Dr Steve Ziola

4. Prof. Daniel J. Collins, Chairman 1
   Code AA/Co
   Department of Aeronautical Engineering
   Naval Postgraduate School
   Monterey, California 93943-5000

5. Prof. Edward M. Wu 4
   Code AA/Wu
   Department of Aeronautical Engineering
   Naval Postgraduate School
   Monterey, California 93943-5000

6. Army Research Office 2
   Engineering and Enviromental Science Division
   Post Office box 12211
   Research Triangle Park, North Carolina 27709-2211
   Attn : Dr Kailasam Iyer

7. Lt Donald A. Gish 2
   3239 Hike's Lane
   Louisville, Kentucky 40220